Gain-of-Function Mutations in *KCNN3* Encoding the Small-Conductance Ca^{2+}-Activated K^+ Channel SK3 Cause Zimmermann-Laband Syndrome

Christiane K. Bauer,[1,*] Pauline E. Schneeberger,[2] Fanny Kortüm,[2] Janine Altmüller,[3,4] Fernando Santos-Simarro,[5] Laura Baker,[6] Jennifer Keller-Ramey,[7] Susan M. White,[8,9] Philippe M. Campeau,[10] Karen W. Gripp,[6] and Kerstin Kutsche[2,*]

Zimmermann-Laband syndrome (ZLS) is characterized by coarse facial features with gingival enlargement, intellectual disability (ID), hypertrichosis, and hypoplasia or aplasia of nails and terminal phalanges. *De novo* missense mutations in *KCNH1* and *KCNK4*, encoding K^+ channels, have been identified in subjects with ZLS and ZLS-like phenotype, respectively. We report *de novo* missense variants in *KCNN3* in three individuals with typical clinical features of ZLS. KCNN3 (SK3/KCa2.3) constitutes one of three members of the small-conductance Ca^{2+}-activated K^+ (SK) channels that are part of a multiprotein complex consisting of the pore-forming channel subunits, the constitutively bound Ca^{2+} sensor calmodulin, protein kinase CK2, and protein phosphatase 2A. CK2 modulates Ca^{2+} sensitivity of the channels by phosphorylating SK-bound calmodulin. Patch-clamp whole-cell recordings of KCNN3 channel-expressing CHO cells demonstrated that disease-associated mutations result in gain of function of the mutant channels, characterized by increased Ca^{2+} sensitivity leading to faster and more complete activation of KCNN3 mutant channels. Pretreatment of cells with the CK2 inhibitor 4,5,6,7-tetrabromobenzotriazole revealed basal inhibition of wild-type and mutant KCNN3 channels by CK2. Analogous experiments with the KCNN3 p.Val450Leu mutant previously identified in a family with portal hypertension indicated basal constitutive channel activity and thus a different gain-of-function mechanism compared to the ZLS-associated mutant channels. With the report on *de novo KCNK4* mutations in subjects with facial dysmorphism, hypertrichosis, epilepsy, ID, and gingival overgrowth, we propose to combine the phenotypes caused by mutations in *KCNH1*, *KCNK4*, and *KCNN3* in a group of neurological potassium channelopathies caused by an increase in K^+ conductance.

Introduction

Zimmermann-Laband syndrome (ZLS [MIM: 135500]) is a rare developmental disorder characterized by facial dysmorphism with bulbous nose and thick floppy ears, gingival enlargement, intellectual disability (ID) with or without epilepsy, hypoplasia or aplasia of terminal phalanges and nails, hypertrichosis, joint hyperextensibility, and hepatosplenomegaly.[1–4] In a proportion of subjects with ZLS, *de novo* missense variants in *KCNH1* (MIM: 603305) has been identified.[5] At the same time, heterozygous *KCNH1* missense variants have been reported in individuals with Temple-Baraitser syndrome (TBS [MIM: 611816]) which shows considerable phenotypic overlap with ZLS.[6] With the identification of additional *KCNH1*-mutation positive individuals, the great clinical variability became apparent;[7–9] however, a core phenotype of severe ID, neonatal hypotonia, hypertelorism, broad nasal tip, wide mouth, nail aplasia or hypoplasia, a proximal implanted and long thumb, and long great toes was defined.[9] *KCNH1* encodes the Eag1 (Kv10.1) channel which belongs to the ether-à-go-go family of voltage-gated K^+ channels. KCNH1 channels show the typical K_v membrane topology, with the six transmembrane domains S1 to S6, a pore lining loop between S5 and S6, and the cytoplasmic C- and N-terminal domains.[10] Electrophysiological studies demonstrated a shift in the activation threshold to more negative potentials and slower deactivation for the KCNH1 mutant channels compared to wild-type KCNH1 indicating a gain-of-function effect for ZLS- and TBS-associated *KCNH1* missense variants.[5,6] Recently, two different *de novo* missense mutations in *KCNK4* (MIM: 605720), encoding a two-pore-domain K^+ channel (K2P), have been reported in three subjects with a consistent phenotype of facial dysmorphism, hypertrichosis, epilepsy, developmental delay/ID, and gingival overgrowth (acronym FHEIG syndrome).[11] KCNK4 (or TRAAK) belongs to the TRAAK/TREK subfamily of lipid- and mechano-sensitive K2P channels.[12] The mutant channels $KCNK4^{Ala244Pro}$ and $KCNK4^{Ala172Glu}$ showed a higher maximal basal activity compared to the wild-type and could not be stimulated further by mechanical stimuli and arachidonic acid, indicating an activating effect of the two disease-associated amino acid substitutions. The clinical features of the *KCNK4*-related condition are reminiscent of ZLS and TBS,[11] providing evidence for a

[1]Department of Cellular and Integrative Physiology, University Medical Center Hamburg-Eppendorf, 20246 Hamburg, Germany; [2]Institute of Human Genetics, University Medical Center Hamburg-Eppendorf, 20246 Hamburg, Germany; [3]Cologne Center for Genomics University of Cologne, 50931 Cologne, Germany; [4]Center for Molecular Medicine Cologne (CMMC), University of Cologne, 50931 Cologne, Germany; [5]Sección de Genética Clínica, Instituto de Genética Médica y Molecular (INGEMM), Hospital Universitario La Paz, IdiPAZ, CIBERER, ISCIII, 28046 Madrid, Spain; [6]Division of Medical Genetics, Alfred I. duPont Hospital for Children, Wilmington, DE 19803, USA; [7]GeneDx, Gaithersburg, MD 20877, USA; [8]Victorian Clinical Genetics Services, Murdoch Children's Research Institute, Royal Children's Hospital, Melbourne, VIC 3052, Australia; [9]Department of Paediatrics, University of Melbourne, Melbourne, VIC 3010, Australia; [10]Department of Pediatrics, Sainte-Justine Hospital, University of Montreal, Montréal, QC H3T 1C5, Canada
*Correspondence: cbauer@uke.de (C.K.B.), kkutsche@uke.de (K.K.)
https://doi.org/10.1016/j.ajhg.2019.04.012.

Figure 1. Clinical Features of the Three Individuals with a *De Novo KCNN3* Variant
(A and B) Subject 1 at age 5 (A) and 46 years (B). He has long and coarse face, bulbous nose and full lips.
(C) At the age 5 years, he had marked gingival enlargement.
(D and E) He has aplastic nails of thumbs and 5th fingers and hypoplastic nails of 2nd to 4th fingers (D). All toes show nail aplasia (E).
(F–H) Subject 2 at age 3 (F and H) and 5 years (G). Her face is coarse, and she has a broad nasal base, tip, and bridge.
(I and J) She has triphalangeal and long thumbs, and her halluces are also long. She has severe nail hypoplasia of the thumbs and mild nail hypoplasia of 2nd to 5th fingers (I). Great toes show nail aplasia and all other toes extreme hypoplasia of nails (J).
(K–M) Subject 3 at age 2.5 (K) and 5.5 (L and M) years. Note broad nasal tip and bridge, long philtrum, and long eye lashes.
(N and O) She has hypoplastic nails of 2nd to 5th fingers that is most severe on 5th fingers (N). All toe nails are hypoplastic (O).

channelopathy caused by hyperactivation of K^+ channels from different subfamilies, including KCNH1 and KCNK4.

Here, we report the identification of dominantly acting missense mutations in *KCNN3* (MIM: 602983) in three subjects with the major clinical features of ZLS and significant clinical overlap with *KCNH1*- and *KCNK4*-related disorders. *KCNN3* codes for one of three members of the small-conductance Ca^{2+}-activated K^+ channels (SK channels) that are widely expressed in the nervous system and important for regulating somatic excitability. SK channels are voltage independent and gated by submicromolar intracellular Ca^{2+} concentrations.[13] KCNN3/SK3 and KCNN2/SK2 channels are part of large multiprotein complexes consisting of the pore-forming channel subunits, the constitutively bound Ca^{2+} sensor calmodulin (CaM), protein kinase CK2, and protein phosphatase 2A (PP2A).[14–16] Binding of Ca^{2+} ions to CaM opens SK channels.[16] CK2 and PP2A further modulate Ca^{2+} sensitivity of the channels by phosphorylating or dephosphorylating SK-bound CaM.[13–15] Our electrophysiological data provide evidence that the disease-associated *KCNN3* mutations increase the Ca^{2+} sensitivity of SK3 channels leading to faster and more complete activation of the mutant channels. Together with the phenotypes associated with activating *KCNH1* and *KCNK4* alleles, the *KCNN3*-related disorder belongs to a channelopathy characterized by DD/ID, coarse face, gingival hyperplasia, and/or nail hypo- or aplasia and caused by dysregulated K^+ channels.

Material and Methods

Study Approval

Informed consent for genetic analyses was obtained from all subjects, and genetic studies were performed clinically or as approved by the Institutional Review Boards of the respective institution. Permission to publish photographs was provided for all subjects shown in Figure 1.

Whole-Exome Sequencing and Sequence Data Analysis

Subject 1

Whole-exome sequencing (WES) was performed on genomic DNA extracted from leukocytes of subject 1 and his healthy parents by the Cologne Center for Genomics (CCG, Cologne, Germany):[17] DNAs were subjected to the standard protocol SureSelectXT Automated Target Enrichment for Illumina paired-end multiplexed sequencing using the Bravo automated liquid handling platform (Agilent). Enrichment was carried out using the SureSelect Human All Exon V6 Kit (Agilent). Each captured library was then loaded and sequenced on the HiSeq 4000 platform (Illumina). Variant analysis was performed as previously described.[18–20] Briefly, the workflow of the Genome Analysis Toolkit (GATK)[21] recommended by the developers was applied. Afterward, variants were functionally annotated and compared to those documented in publicly accessible genetic variant databases (dbSNP138, 1000 Genomes, and ExAC) using AnnoVar (v2015-03-22).[22] Only private (absent in public database) and rare (with a minor allele frequency <0.5% and not present in the homozygous state in public databases or the parents) exonic and intronic variants at exon-intron boundaries ranging from −40 to +40 were retained. The *KCNN3* variant c.1306A>T predicting the amino acid change p.Ser436Cys (according to mRNA reference sequence GenBank: NM_002249.6) was confirmed to be *de novo* by Sanger sequencing.

Subject 2

WES in the proband was performed using SureSelect Exon Capture v4 (Agilent) and paired-end sequencing on a HiSeq2500 (Illumina). The data output of the Illumina sequencer Hiseq2500 FASTQ files were converted by the CASAVA v1.8 software (Illumina) and the sequences aligned to the reference human genome (GRCh37) with the Burroughs-Wheeler algorithm (BWA), followed by a local alignment for indels with the Broad Institute Genome Analysis Tool Kit (GATK). Duplicated sequences were removed with the tool Picard. The identification of variants was made with the GATK Unified Genotyper module and then annotated with Annovar. Exome variants were filtered for coding and splicing variants with a minor allele frequency of <0.5% in the Exome Variant Server. After analyzing the exome for known disease genes involved in disorders with an overlapping phenotype and finding no candidate, the candidate gene *KCNN3* was discussed between K.K. and P.M.C., and Sanger sequencing of the variant c.805A>G (p.Lys269Glu) in healthy parents using standard techniques demonstrated it to be *de novo*.

Subject 3

Using genomic DNA from the proband and parents, the exonic regions and flanking splice junctions of the genome were captured using the Clinical Research Exome kit (Agilent Technologies) or the IDT xGen Exome Research Panel v1.0. Massively parallel (NextGen) sequencing was done on an Illumina system with 100 bp or greater paired-end reads. Reads were aligned to human genome build GRCh37/UCSC hg19 and analyzed for sequence variants using a custom-developed analysis tool. Additional sequencing technology and variant interpretation protocol has been previously described.[23] The general assertion criteria for variant classification are publicly available on the GeneDx ClinVar submission page.

Plasmids and Mutagenesis

Human *KCNN3* (GenBank: NM_002249.6) in pEGFP-N1 was a kind gift from Prof. Dr. Stephan Grissmer (Institute of Applied Physiology, Ulm University). The coding region of *KCNN3* was amplified and the PCR product was cloned into pENTR/D-TOPO vector (ThermoFisher) according to the manufacturer's protocol. The mutations c.805A>G, c.1049G>A, c.1306A>T, and c.1348G>C were introduced by using the Quik Change II Site Directed Mutagenesis Kit (#200523; Agilent) according to manufacturer's instructions. Subsequently, these constructs were used for transferring the coding region into GATEWAY-compatible destination vectors pRK5-Myc-D3-DEST, pMT2SM-HA-DEST, and pcDNA3-DEST with the Gateway LR Clonase II Enzyme Mix (#11791; Invitrogen). *CALM3* (encoding CaM; GenBank: NM_005184.3) in pEYFP (EYFP-hCaM) was a gift from Emanuel Strehler[24] (Addgene plasmid #47603) and was used directly for transfection. pZW6 (CK2α-HA) and pZW12 (Myc-CK2β) were a gift from David Litchfield[25] (Addgene plasmids #27086 and #27088) and were used either directly for transfection (pZW12) or as a template (pZW6) for cloning the coding region of CK2α into pFLAG6-N3 with the In-Fusion HD Cloning Kit (Takara) according to the manufacturer's protocol. All constructs were regularly sequenced for integrity.

Co-immunoprecipitation

HEK293T cells (CRL-3216; ATCC) were cultured and transiently transfected as described previously.[20] For detection of phosphorylated CaM, cells were incubated with PBS or PBS+/+ (PBS supplemented with 0.9 mM $CaCl_2$, 0.52 mM $MgCl_2$, and 0.16 mM $MgSO_4$) for 30 min at 37°C before lysis. Cells were lysed in ice-cold co-immunoprecipitation buffer (IP buffer) (120 mM NaCl, 50 mM Tris/HCl [pH 8], 0.5% Nonidet P40, 1 mM EDTA, or 10 μM $CaCl_2$ as indicated in the respective experiment, and supplemented with complete Mini Protease Inhibitors and PhosSTOP [Roche]), and cell lysates were clarified by centrifugation for 10 min at 4°C. After taking a total cell lysate control (input), supernatants were transferred to 20 μL GFP-Trap A beads (Chromotek) or 30 μL Pierce anti-c-Myc Magnetic Beads (ThermoFisher Scientific) and incubated for 2 h at 4°C under rotating conditions. Precipitates were collected by repeated centrifugation and washing with lysis buffer (2,500 × *g*; 2 min; 4°C) or with a magnetic stand and washing under rotating conditions at room temperature for 3 min. After final washing, beads were resuspended in 4× sample buffer (33% glycerol, 80 mM Tris-HCl [pH 6.8], 0.3 M DTT, 6.7% sodium dodecyl sulfate, 0.1% bromophenol blue) and the supernatant was subjected to SDS-PAGE and immunoblotting.

Western Blot Analysis

Protein extracts were separated on SDS-PAGE under denaturing conditions and transferred to PVDF (polyvinylidene fluoride) membranes. Membranes were blocked with 5% non-fat dry milk in TBST or 5% bovine serum albumin (BSA) in TBST followed by incubation with the indicated primary antibody overnight at 4°C and by horseradish peroxidase (HRP)-linked secondary antibodies at room temperature for 1 h. Chemiluminescent western blots were digitally imaged using a ChemiDoc MP (Bio-Rad).

Antibodies

The following primary antibodies and dilutions were used: rabbit polyclonal anti-phospho Calmodulin Thr79+Ser81 antibody (1:500; ab194526; Abcam), mouse monoclonal anti-FLAG horseradish peroxidase (HRP)-coupled antibody (1:40,000; A8592; clone M2, Sigma-Aldrich), mouse monoclonal purified anti-GFP Epitope Tag antibody (1:5,000; #902601; clone B34; BioLegend), rat monoclonal anti-HA HRP-coupled antibody (1:5,000; #12013819001;

clone 3F10; Roche), mouse monoclonal anti-Myc HRP-coupled antibody (1:5,000; #1814150; clone 9E10; Roche), and mouse monoclonal anti-α-Tubulin antibody (1:10,000; #T9026; clone DM1A; Sigma-Aldrich). The following secondary antibodies and dilutions were used: sheep anti-mouse IgG HRP-coupled antibody (1:10,000; #NA931V; GE healthcare) and donkey anti-rabbit IgG HRP-coupled $F(ab')_2$ fragment (1:5,000; #NA9340V; GE healthcare).

Data Analysis and Statistics of Biochemical Experiments

Band intensities of immunoblots were determined using the Image Lab v6.0 software (Bio-Rad). Quantitative data are presented as the mean ± standard deviation (SD) performed by GraphPad prism8 software (Instat, GraphPad Software). For biochemical experiments shown in Figures S1 and S2, statistical analysis was performed by using one-way analysis of variance ANOVA followed by a Dunnett post hoc test for multiple comparison. For biochemical experiments shown in Figure S8, differences between two groups were analyzed with an unpaired t test. A p value of less than 0.05 was considered statistically significant ($*p \leq 0.05$). *F* values and degrees of freedom are provided.

Electrophysiology

For heterologous expression of KCNN3 channels, Chinese hamster ovary (CHO) cells were transfected with a wild-type (WT) or mutant human *KCNN3* cDNA construct (in pcDNA3-DEST; Invitrogen) and a plasmid expressing EGFP (pEGFP-N1; Clontech) using LipofectAMINE 2000 (Invitrogen). Final concentration of the channel plasmid was 0.8 μg/mL (standard) or 4 μg/mL ("ATP" experiments). Patch-clamp experiments were performed 1 to 2 days after CHO cell transfection using the conventional whole-cell configuration of the patch-clamp technique. In addition, some data were recorded with the cell-attached configuration. The external Ringer solution contained 140 mM NaCl, 5 mM KCl, 0.8 mM $MgCl_2$, 1 mM $CaCl_2$, 2.5 mM EGTA, 5 mM glucose, and 10 mM HEPES; pH adjusted to 7.4 with NaOH. The nominal free Ca^{2+} concentration of the external solution amounted to 50 nM. All given nominal free Ca^{2+} concentrations were calculated with the Maxchelator program Ca-Mg-ATP-EGTA Calculator, V1.0, NIST database #46 v8. The "standard" pipette solution with a nominal free Ca^{2+} concentration of 1 μM (see also Fanger et al.[26]) contained 130 mM K^+ aspartate, 2.08 mM $MgCl_2$, 8.55 mM $CaCl_2$, 10 mM EGTA, and 10 mM HEPES. The "4 mM ATP" pipette solution with a nominal free Ca^{2+} concentration of 300 nM contained 130 mM K^+ aspartate, 4 mM $MgCl_2$, 6.346 mM $CaCl_2$, 10 mM EGTA, 10 mM HEPES, and 4 mM Na_2-ATP (added prior to use). The pH of the pipette solutions was adjusted to 7.2 with KOH yielding a final K^+ concentration of about 160 mM. Experiments were performed at 20°C–22°C. External solutions with the membrane-permeable casein kinase 2alpha inhibitor TBB (4,5,6,7-tetrabromobenzotriazole; sc-202830; Santa Cruz Biotechnology) were freshly prepared before application using stocks of 10 mM TBB dissolved in DMSO and stored at −20°C; the final bath concentration of TBB was 5 μM.

Patch pipettes had resistances of 3.6 to 4.0 MΩ when filled with the standard low chloride solution. The access resistance in the whole-cell configuration was mostly in the range of 5 to 6 MΩ. If possible, series resistance was compensated for by at least 70% and no leak subtraction was performed. Data were corrected online for a liquid junction potential of about −13 mV for an aspartate-based solution. An EPC-9 patch clamp amplifier was used in combination with the PATCHMASTER stimulation and data acquisition software (HEKA Elektronik).

Data Analysis of Electrophysiology Experiments

Patch-clamp data processing was performed with FITMASTER (HEKA), Excel (Microsoft Corp.), and Sigmaplot 11.0 (Systat Software). Whole-cell membrane currents recorded with a voltage ramp protocol were analyzed with respect to current amplitudes at 0 mV ramp potential, determined as mean value between −4 and +4 mV ramp potential. The time course of current amplitudes at 0 mV after establishment of the whole-cell configuration was traced with voltage ramps applied every 5 s. The time of the first measurement was defined as $t = 5$ s. Two parameters served to characterize the time course of KCNN3 channel activation up to a first saturation of current amplitudes. (1) The current amplitude determined at $t = 10$ s relative to the current amplitudes attained after (the first) saturation of KCNN3 currents. Since WT and KCNN3 p.Val450Leu mutant channels tended to show variably delayed further changes in current amplitudes, the period up to the first saturation of current amplitudes was defined as 1st phase of channel activation. (2) The time to reach at least 70% of the maximal current amplitude within the 1st phase of channel activation. In addition, the reversal potential was measured, since high K^+ conductance shifts the reversal potential to the K^+ equilibrium potential and a reduced seal resistance is indicated by a drop in the reversal potential (change to less negative values). The value of the reversal potential was determined as the ramp potential with the first reversal from inward to outward current. In the cell-attached mode, conductance values were determined as I/V slope between −88 and −72 mV ramp potential. Whole-cell experiments were performed in two separate main sets to enable closely parallel experiments on WT and mutant KCNN3 channels with identical batches of cells and solutions. In the first set of whole-cell experiments (WT, p.Lys269Glu, and p.Gly350Asp KCNN3 channels), 1 s voltage ramps (160 mV/s) were used, and in the second set of experiments (WT, p.Ser436Cys, and p.Val450Leu), 100-ms voltage ramps (160 mV/0.1 s) were mostly used, since the steepness of the voltage ramp was found to have only marginal effects on the shape of the recorded currents. The effect of acute application of the CK2 inhibitor TBB on WT and mutant KCNN3 channels was determined as ratio of current amplitudes at 0 mV, $I_{TBB} / I_{control}$, where I_{TBB} is the maximal current amplitude measured within 150 s after TBB application and $I_{control}$ is the current amplitude just before TBB application. The period of 150 s represents a compromise between missing possibly delayed TBB effects and mistakenly attributing spontaneously occurring increases in Ca^{2+} sensitivity to the TBB effect.

Experimental data are presented as boxplot (Cleveland method; boxes indicate the 25% to 75% range, whiskers the 10/90 percentiles, and points the 5/95 percentiles; the median is shown as line). 5/95 percentiles are missing if $n < 10$, with n representing the number of experiments from different cells. Statistical testing was performed with Sigmaplot 11.0 and Sigmaplot 13.0 using a significance level α of 0.05. Differences between two groups were analyzed with the Wilcoxon-Mann-Whitney test. For comparisons of three groups, the Kruskal-Wallis test (ANOVA on ranks) was used with post hoc Dunn's test to identify the significantly differing groups. If significant differences were found between channel mutants and WT data, the individual significance level was determined with the Wilcoxon-Mann-Whitney test.

Results

Identification of *De Novo KCNN3* Missense Mutations in Three Subjects with a Phenotype Resembling ZLS

We investigated a 46-year-old male (subject 1) with the clinical diagnosis of ZLS. He had mild to moderate intellectual disability, a long and coarse face with a bulbous nose, marked gingival enlargement, hypoplasia of the distal phalanges of hands and feet, aplasia or hypoplasia of finger and toe nails, and moderate hypertrichosis from birth (Figure 1 and Table 1). Sanger sequencing of *KCNH1* and *ATP6V1B2* did not reveal a sequence variant of pathogenic relevance (data not shown). Analysis of trio WES data was performed according to an X-linked, autosomal-recessive, and autosomal-dominant inheritance model, the latter with a *de novo* mutation in subject 1. We identified the *de novo* variant c.1306A>T in *KCNN3* predicting the amino acid change p.Ser436Cys (Figure 2, Tables 1 and S1). The variant was absent in dbSNP138, 1000 Genomes Project, Exome Variant Server, and ExAC and gnomAD browsers (Table S1), and *de novo* occurrence was confirmed by Sanger sequencing. Through an international collaboration and GeneMatcher,[30] we identified two additional individuals with a *de novo* event in *KCNN3* (Figure 1). In subject 2 the missense variant c.805A>G (p.Lys269Glu) and in subject 3 the non-synonymous change c.1049G>A (p.Gly350Asp) were detected (Tables 1 and S1); both variants were confirmed to be *de novo* by Sanger sequencing. Trio WES in subjects 1 and 3 did not reveal additional *de novo* variants; the single whole exome in subject 2 did not allow for filtering *de novo* variants. Subjects 2 and 3 were 4.5 and 5.5 years old, respectively, and shared a phenotype including coarse facial features, developmental delay, hypotonia, short distal phalanges, hypoplasia/aplasia of nails on hands and feet, and patent ductus arteriosus suggestive of ZLS (Figure 1 and Table 1). Besides coarse facial features, we specifically noticed a broad nasal tip and triangular nostrils in the three subjects (Figures 1A, 1B, 1F, 1G, and 1K). The two variants had not been reported in ExAC and gnomAD (Table S1). All three pathogenicity prediction algorithms predicted the three KCNN3 amino acid substitutions p.Lys269Glu, p.Gly350Asp, and p.Ser436Cys to have a damaging impact on protein function (Table S1). The three affected residues are evolutionarily highly conserved in orthologs, and two amino acids (glycine 350 and serine 436) are invariant in KCNN1, KCNN2, and KCNN4, three other members of the KCNN family (Figure 2A). With a Z score of 4.18, *KCNN3* is intolerant to functional genetic variation,[31] further indicating a pathogenic role of the *KCNN3* variants in the affected individuals. Four members of a published family, a father and three children, carried the heterozygous *KCNN3* variant c.1348G>C (p.Val450Leu) and were diagnosed with idiopathic non-cirrhotic portal hypertension (INCPH). Testing of the affected father's healthy parents showed the variant to be *de novo* in the father. The authors speculated that specific *KCNN3* variants may affect endothelial vasoregulation in the portal vein, hepatic artery, or sinusoids and play a pathogenic role in INCPH. However, electrophysiological studies have not been performed to investigate the effect of the p.Val450Leu change on KCNN3 channel function.[32]

Identified *KCNN3* Mutations in Relation to Structure-Function of KCNN Channels

The three SK family members share the typical serpentine transmembrane topology with six transmembrane domains and cytosolic N and C termini (Figure 2B).[13] Recently, the structure of the human homotetrameric KCNN4 channel in closed and activated states has been determined by cryo-electron microscopy.[27] Based on this available structure (KCNN4 in the Ca^{2+}-free state), we obtained the presumed structure of KCNN3 shown in Figure 2B. The ion channel pore is formed by transmembrane helices S5 and S6 and surrounded by membrane-embedded helices S1 to S4. The S4-S5 linker consists of two α helices, $S_{45}A$ and $S_{45}B$ (Figure 2B). $S_{45}A$ binds CaM, but only the N-terminal lobe of CaM.[27] The C-terminal end of the SK4 channel forms three helices: HA and HB, the two intracellular helices which constitutively bind the C-lobe of CaM, are oriented almost parallel to the membrane, and the HC helices of four channel subunits are located at the center (Figure 2B).[27] The three amino acid residues mutated in individuals with a ZLS-like phenotype (p.Lys269Glu, p.Gly350Asp, and p.Ser436Cys) are located close to each other in the cytoplasmic space (Figure 2B). Lys269 is located in the N terminus of KCNN3 (Figures 2A and 2B). Mutation of lysine to alanine at position 121 in SK2/KCNN2 (lysine 120 in KCNN2 and lysine 269 in KCNN3 in Figure 2A) has been shown to increase the deactivation time constant and to cause a left-shift in the Ca^{2+} sensitivity of the KCNN2 mutant channel.[14] Accordingly, we hypothesized that the p.Lys269Glu change may similarly increase the apparent Ca^{2+} sensitivity of the KCNN3 mutant channel. Glycine 350 in KCNN3 is analogous to glycine 92 in KCNN4 and located in the cytoplasmic linker between S2 and S3 (Figures 2A and 2B). In KCNN4, the cytosolic portion of the S2 helix is in direct contact with CaM; whether glycine 92 is important for the contact between S2 of KCNN4 and CaM is not known.[27] Serine 181 in KCNN4, which corresponds to serine 436 in KCNN3, is located in the $S_{45}A$ helix (Figures 2A and 2B) and in direct contact with the CaM N-lobe pocket. By mutating serine 181 in KCNN4, the proposed interaction between the $S_{45}A$ helix and the CaM N-lobe and its role in KCNN4 channel opening has been demonstrated.[27] Together, structural data from KCNN4 imply that the three KCNN3 amino acid substitutions identified in ZLS-affected individuals are located at structurally and functionally relevant positions and may have an impact on KCNN3 channel gating. The valine-to-leucine change at position 450 previously identified in a family with INCPH[32] affects a highly conserved amino

Table 1. Clinical Features of Subjects with a Heterozygous *KCNN3* Missense Variant

Subject #	1	2	3	Published Family (Koot et al.[32])			
Mutation (NM_002249.6; NP_002240.3)	c.1306A>T (p.Ser436Cys)	c.805A>G (p.Lys269Glu)	c.1049G>A (p.Gly350Asp)	c.1348G>C (p.Val450Leu)			
Exon	3	1	3	3			
Origin	*de novo*	*de novo*	*de novo*	*de novo*	inherited		
Nationality	white (Australian)	white (Spanish)	white (USA)	unknown			
Sex	M	F	F	M	M	F	F
Age[a]	46 y	4.5 y	5.5 y	37 y	10 y	1 y	2 y
Birth weight (SD)	3,800 g (42 wks) (0)	3,800 g (38 wks) (+1.5)	3,392 g (39 wks) (0)	ND	ND	ND	ND
Birth length (SD)	ND	52 cm (+0.7)	50.8 cm (+0.4)	ND	ND	ND	ND
OFC birth (SD)	36 cm (−0.1)	38 cm (+2.9)	35 cm (−0.4)	ND	ND	ND	ND
Weight[a] (SD)	95.7 kg (+2)	15.5 kg (−0.9)	30.7 kg (+2.4)	ND	ND	ND	ND
Height[a] (SD)	172 cm (−1.3)	99 cm (−1.7)	113 cm (+0.2)	ND	ND	ND	ND
OFC[a] (SD)	57.5 cm (+0.3)	52 cm (+1.3)	52.9 cm (+1.7)	ND	ND	ND	ND
DD/ID	mild to moderate ID	DD with walking independently at 2 y; first words with 2.5 y; attends nursery; difficulties in gross motor coordination	DD with walking independently at 18 mo; limited spoken language; attends school with a personal aide	ND	mild pervasive developmental disorder	ND	ND
Tonus	normal	hypotonia	low tone centrally; increased tone in lower extremities and toe walking	ND	ND	ND	ND
Seizures	no	no	no	ND	ND	ND	ND
EEG	ND	normal	largely normal	ND	ND	ND	ND
MRI scan	ND	normal	normal	ND	ND	ND	ND
Hearing	normal	normal evoked potential; sometimes complains of hyperacusis	normal	ND	ND	ND	ND

(*Continued on next page*)

Table 1. ***Continued***

Subject #	1	2	3	Published Family (Koot et al.[32])			
Eye findings	normal	wears glasses due to hypermetropia	elevated optic disc bilaterally without cupping; OCT showed normal retinal nerve fiber layer	ND	ND	ND	ND
Craniofacial dysmorphism	long and coarse face; bulbous nose (several reduction surgeries); full lips; high arched palate	coarse face; plagiocephaly; thick lower vermillion; broad nasal tip; thick alae nasi; broad nasal base and bridge; narrow forehead	slightly prominent and cupped ears; very long eye lashes; very broad nasal tip; long philtrum	ND	ND	ND	ND
Gingival enlargement	marked (several surgical reductions)	mild	no	ND	ND	ND	ND
Skeletal abnormalities of hands and feet	short fingers and toes; hypoplasia of distal phalanges of hands and feet	short distal phalanges; short 1st metacarpal; long thumbs and halluces; triphalangeal thumbs; clinodactyly	hands: bilateral contractures, distal digital hypoplasia; fingers very tapered; thumbs grossly normal; feet: toes essentially normal appearing; radiographs of hands: dysmorphic and hypoplastic distal phalanges, pronounced anomalies involving 5th fingers and thumbs; radiographs of toes: distal phalanx of great toes is shortened and dysmorphic; punctate distal phalanges in middle and 4th toes; no distal phalanges seen in the 2nd and 5th toes	ND	ND	ND	ND
Aplastic or hypoplastic nails	hands: aplastic nails of thumbs and 5th fingers; hypoplastic nails of 2nd–4th fingers; feet: aplastic nails of all toes	hands: severe nail hypoplasia of the thumb and mild hypoplasia of 2nd–5th fingers; feet: nail aplasia of the hallux and extreme hypoplasia of 2nd–5th toe	hand: hypoplastic nails of 2nd–5th fingers; mostly strikingly on 5th fingers; feet: hypoplastic nails of all toes	ND	ND	ND	ND
Scoliosis	no	dorso-lumbar kyphosis	no	ND	ND	ND	ND

(*Continued on next page*)

Table 1. ***Continued***

Subject #	**1**	**2**	**3**	**Published Family (Koot et al.[32])**			
Hypertrichosis	moderate hypertrichosis on trunk and limbs since birth	thick eyebrows; mild synophrys; prominent eyelashes; low anterior hairline; thick hair	very long eye lashes; very mild facial hypertrichosis with synophrys	ND	ND	ND	ND
Liver findings	liver function normal; abdominal ultrasound shows features consistent with fatty liver disease	liver function normal; abdominal ultrasound normal	liver enzymes normal	INCPH: splenomegaly; portal hypertension; no signs of cirrhosis, portal vein thrombosis or Budd-Chiari syndrome	INCPH: hepatomegaly and segmental portal vein thrombosis; prominent portal hypertension	INCPH: hepatosplenomegaly; portal hypertension; no signs of cirrhosis; portal vein thrombosis or Budd-Chiari syndrome	INCPH: hepatomegaly; portal hypertension; no portal vein thrombosis or signs of cirrhosis
Other anomalies	inguinal hernia repair; parental concern regarding memory loss in fourth decade of life but no documented cognitive regression; episode of possible psychosis aged 43 which was treated with anti-psychotic medication	patent ductus arteriosus (surgically corrected at 4 mo); right supernumerary nipple; unexplained polycythemia	patent ductus arteriosus (closed spontaneously); bifid uvula	pneumococcal peritonitis at age 1 y	ND	pneumococcal sepsis at age 7 mo	ND

Abbreviations: DD, developmental delay; F, female; ID, intellectual disability; INCPH, idiopathic non-cirrhotic portal hypertension; M, male; mo, months; ND, no data; OCT, optical coherence tomography; OFC, occipito-frontal head circumference; wks, weeks; y, years.
[a]At last examination

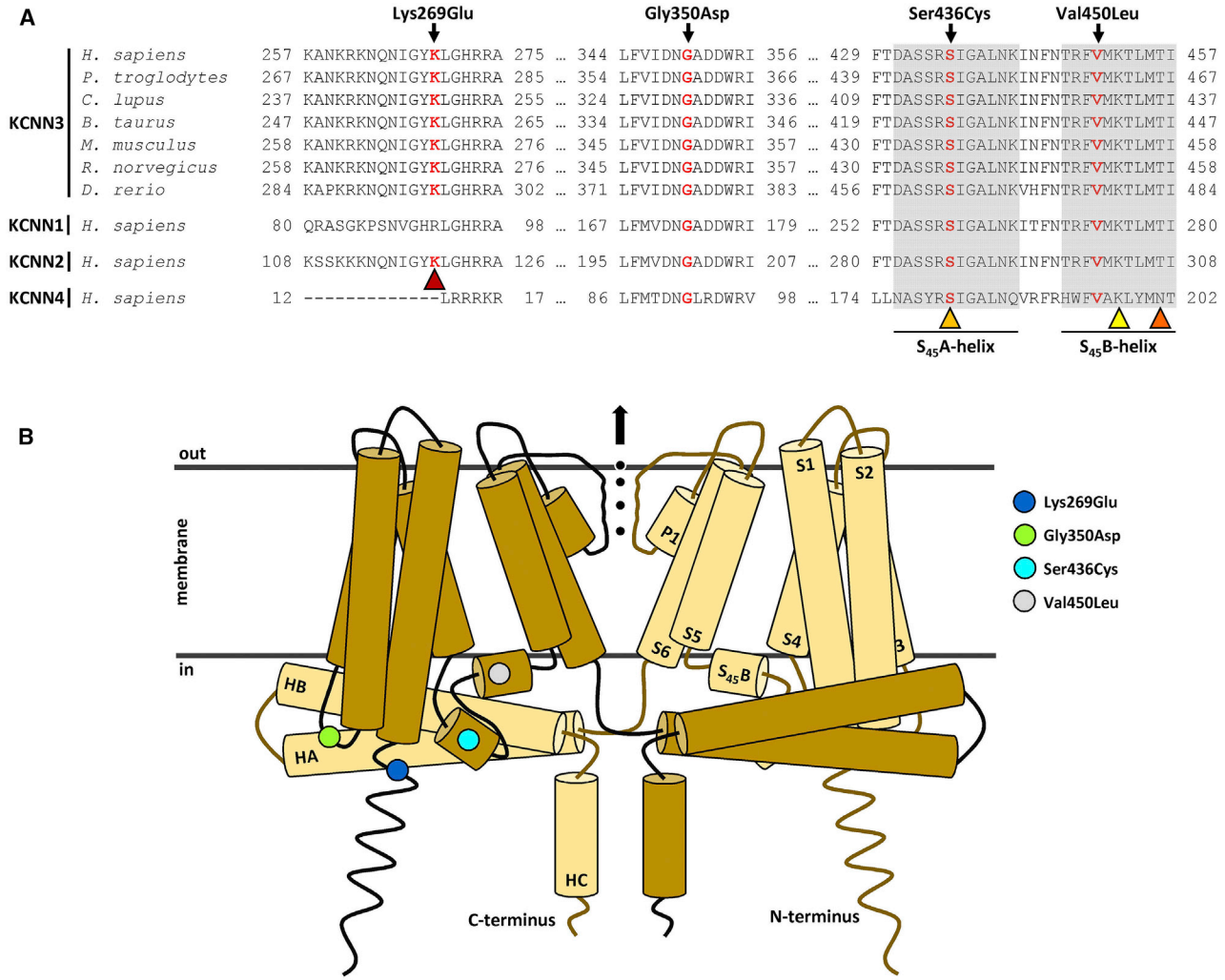

Figure 2. KCNN3 Structure and Partial Protein Sequence Alignments of SK Family Members and KCNN4

(A) Partial amino acid sequence alignment of human KCNN3 (GenBank: NP_002240.3) with orthologs and paralogs (KCNN1 [GenBank: NP_002239.2], KCNN2 [GenBank: NP_067627.2], and KCNN4 [GenBank: NP_002241.1]) shows evolutionary conservation of the mutated residues (highlighted in red) between species and within the human KCNN family. Amino acid residues forming the linker-helices $S_{45}A$ and $S_{45}B$ are shaded in gray and are underlined. Amino acid residues with important functions are indicated by colored triangles: red, possible activation of CK2;[14] light orange, interaction with calmodulin; yellow, intermonomeric interaction; dark orange, intramonomeric interaction.[27] For the alignment the following protein sequences were used: *Homo sapiens* (GenBank: NP_002240.3), *Pan troglodytes* (GenBank: XP_003308520.2), *Canis lupus* (GenBank: XP_547563.2), *Bos taurus* (GenBank: XP_003585876.1), *Mus musculus* (GenBank: NP_536714.2), *Rattus norvegicus* (GenBank: NP_062188.2), *Danio rerio* (GenBank: XP_001921794.2), *Homo sapiens* KCNN1 (GenBank: NP_002239.2), KCNN2 (GenBank: NP_067627.2), and KCNN4 (GenBank: NP_002241.1). Alignment was generated using MUSCLE v3.8.[28] Lysine 121 in KCNN2 reported by Allen et al.[14] corresponds to lysine 120 in KCNN2 according to the reference number GenBank: NP_067627.2 used here.

(B) KCNN3 is a homomeric tetramer; the schematic structure of two opposing monomers (yellow and brown) is shown. The three-dimensional structure of the KCNN3 monomer was obtained by means of homology modeling with the web-based service SWISS-MODEL.[29] The crystallographic structure of KCNN4 in the Ca^{2+}-free state (PDB: 6CNM) at 3.4 Å resolution was used as a template.[27] Each subunit comprises six transmembrane helices (S1 to S6), one pore domain (P1) constituting the selectivity filter, two linker-helices ($S_{45}A$ and $S_{45}B$), and three intracellular helices (HA, HB, and HC). The pore of the KCNN3 tetramer is formed by helices S5 and S6 and is extended by helix HC of each subunit. Locations of mutated residues are indicated by colored dots; the color code for each amino acid substitution is provided on the right. Potassium ions are highlighted as black dots.

acid residue in the $S_{45}B$ helix (Figure 2A). In KCNN4, $S_{45}B$ interacts with S6 from the same and a neighboring subunit to ensure inter-subunit connectivity. Lysine 197 and asparagine 201 in $S_{45}B$ of KCNN4 are important for these inter- and intramonomeric interactions (Figure 2A),[27] suggesting that the KCNN3 substitution p.Val450Leu (corresponding to valine 195 in $S_{45}B$ of KCNN4) at the interface between $S_{45}B$ and S6 helices may destabilize the connectivity between the subunits. To assess this, we performed co-immunoprecipitation experiments with HEK293T cells ectopically expressing wild-type Myc-tagged KCNN3 and either of the four HA-tagged mutant channel subunits. While complex formation between KCNN3 wild-type and the three ZLS-associated KCNN3 mutants was comparable

to that of KCNN3 wild-type channel subunits among themselves (Figure S1), the amount of co-IPed KCNN3 Val450Leu mutant channel subunit with Myc-KCNN3 wild-type was significantly reduced by ~23% (Figure S1). These data suggest that the four mutations do not have a major impact on KCNN3 subunit interaction, although p.Val450Leu seems to have a slightly negative impact on subunit connectivity.

A prerequisite for functional SK channels is their constitutive CaM binding.[16] To analyze the effect of the mutations on the interaction of KCNN3 with CaM, we co-expressed HA-tagged wild-type KCNN3 or one of the four mutant channels in HEK293T cells with EYFP-CaM, precipitated EYFP-CaM in IP buffer containing 10 μM $CaCl_2$ and detected the channel in the immunoprecipitates (Figure S2). Wild-type and the four mutant KCNN3 channels were efficiently co-immunoprecipitated with CaM (Figure S2), suggesting that the disease-associated *KCNN3* mutations, including p.Val450Leu, do not significantly affect complex formation between the K^+ channel and CaM.

Functional Expression and Differences between Wild-Type and Mutant KCNN3 Channel Activation

The impact of the different *KCNN3* mutations, including p.Val450Leu, on Ca^{2+}-induced channel activation was investigated by heterologous expression in the mammalian CHO cell line. Electrophysiological experiments were performed in intact cells in the whole-cell configuration of the patch-clamp technique using a near physiological K^+ gradient. K^+ channel activation was traced by applying voltage ramps every 5 s. The wild-type (WT) and all mutant KCNN3 channels were activated by the delivery of Ca^{2+} via the patch pipette demonstrating functional expression of all KCNN3 channels (Figure 3A). The time course of channel activation after access to the cell interior varied considerably, not only for an individual KCNN3 channel type, but also between WT channels and the three KCNN3 mutants p.Lys269Glu, p.Gly350Asp, and p.Ser436Cys, which exhibited a significantly faster saturation of K^+ current amplitudes. The relative current levels attained after 10 s ($I_{10\ s}$) and the time needed to reach 70% of the current amplitude at the first apparent saturation of channel activation ($t_{70\%}$) were used for statistical analysis of the course of channel activation (Figures 3B–3D). Also, p.Val450Leu channels showed significantly increased $I_{10\ s}$ values, whereas the decrease in the median $t_{70\%}$ compared to WT data failed to reach significance in the ANOVA statistical analysis ($p = 0.053$) due to the significantly greater effect of the p.Ser436Cys mutation (Figures 3C and 3D). Consequently, the direct comparison of p.Val450Leu with WT $t_{70\%}$ data yielded a significant difference ($p = 0.006$; Mann-Whitney test). For each channel type, the saturating current levels varied considerably, and even the distribution of current amplitudes determined for WT channels differed between the two sets of experiments. Lower WT current amplitudes in the second set of experiments were associated with significant differences compared to the current levels of p.Ser436Cys and p.Val450Leu mutant channels (Figure S3). Experiments with prolonged recording time revealed further prominent changes in the activation level of WT and p.Val450Leu channels where the last recorded current amplitudes always exceeded the first saturation level (Figure S4). These "late" or "delayed" changes in current amplitude may result from changes in the apparent Ca^{2+} sensitivity of the KCNN3 channels, which might be elicited by washout of cytosolic substances like ATP. Similarly, a faster time course of the initial channel activation after breakthrough to the whole-cell configuration is expected to mirror a higher apparent Ca^{2+} sensitivity.[33]

Effects of CK2 Inhibition on the Course of KCNN3 Channel Activation and Current Amplitudes

The Ca^{2+} sensitivity of SK channels depends on the degree of CK2-dependent phosphorylation of channel-bound CaM.[14,15] Therefore, we investigated the effect of CK2 inhibition on WT and mutant KCNN3 channels. As shown in Figures 4A and 4B, pre-incubation of the cells with the membrane-permeable CK2-specific inhibitor 4,5,6,7-tetrabromobenzotriazole (TBB) drastically accelerated channel activation, resulting in median $I_{10\ s}$ values above 90% for WT, p.Gly350Asp, p.Ser436Cys, and p.Val450Leu channels (all $p \leq 0.001$ compared to the corresponding control values). The time course of p.Lys269Glu KCNN3 channel activation was also significantly accelerated (median $I_{10\ s}$ in TBB: 87.2%, control: $I_{10\ s} = 34.1\%$; $p < 0.001$). These data revealed basal inhibition of wild-type and mutant KCNN3 channels by CK2 in intact cells and suggest that CK2-dependent regulation of Ca^{2+} sensitivity is preserved in all KCNN3 mutants investigated.

Paralleling the similarity in the faster channel activation in the presence of TBB, current amplitudes measured for these highly Ca^{2+}-sensitive KCNN3 channels did not differ significantly between WT and mutant channels (Figures 4B and 4C). For WT channels, the median current amplitude measured after TBB pre-incubation significantly exceeded the corresponding control values (series 1: $p = 0.007$; series 2: $p < 0.001$; control values given in Figure S3) determined after the first saturation of current amplitude. For p.Val450Leu channels, the increase in median current amplitude (in TBB versus control) was not significant ($p = 0.054$), and the other three channel mutants showed no significant change in current amplitude (data in Figures 4C and S3). Remarkably, pre-incubation with TBB was unable to eliminate the very high variability in maximal current amplitudes observed for each channel type (Figure 4C), suggesting that the number of functional membrane-inserted KCNN3 channels differed considerably between the recorded cells. This could be due to fast KCNN3 channel internalization and recycling mechanisms.[34,35]

In another series of experiments, TBB was applied after saturation of channel activation. For all mutant channels, the response to CK2 inhibition was significantly impaired compared to the effects of TBB application on WT

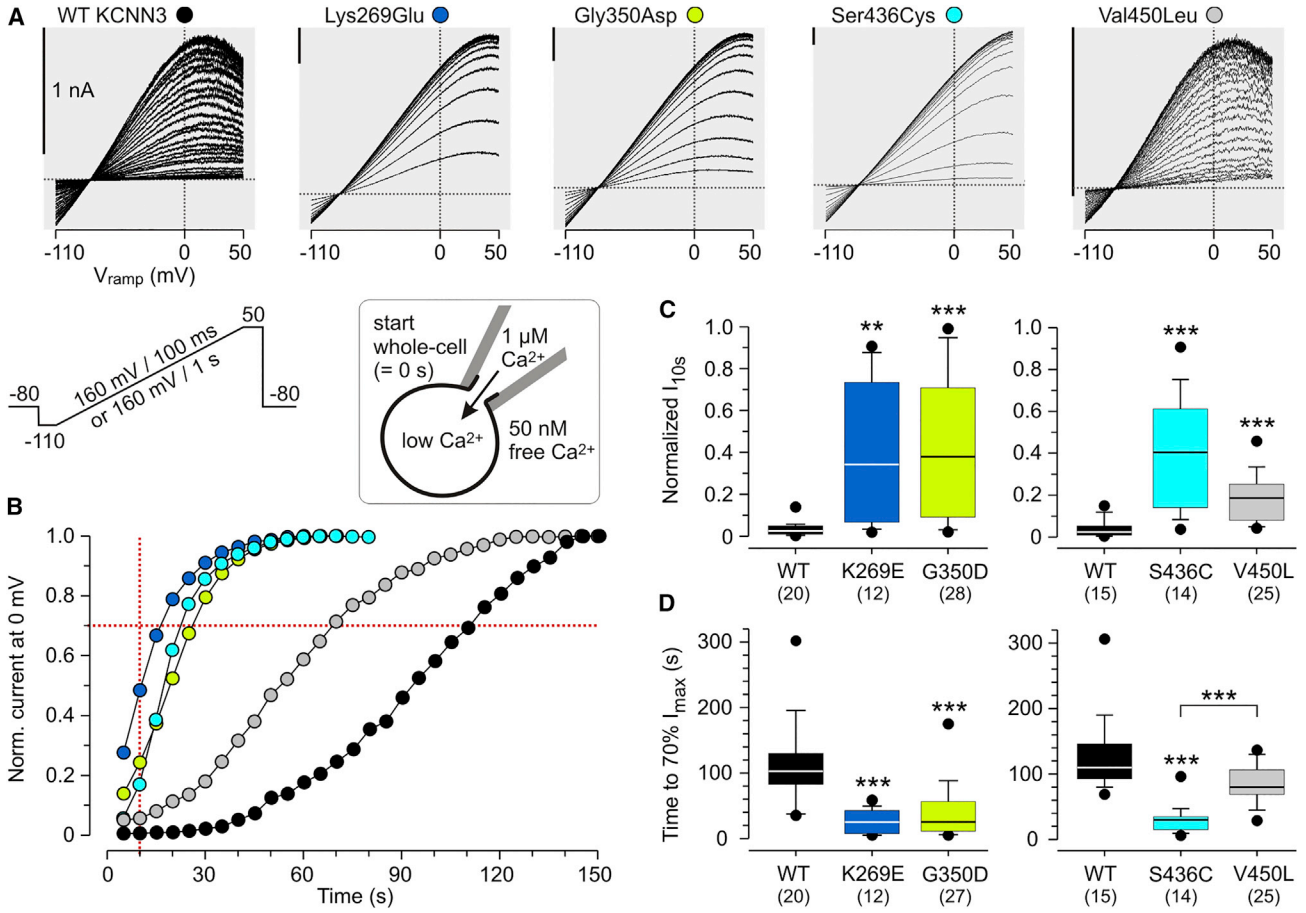

Figure 3. Functional Expression of Wild-Type (WT) and Mutant KCNN3 Channels in CHO Cells Reveals Differences in the Course of Channel Activation

Whole-cell recordings were performed on CHO cells heterologously expressing wild-type (WT), p.Lys269Glu (K269E), p.Gly350Asp (G350D), p.Ser436Cys (S436C), or p.Val450Leu (V450L) KCNN3 channels. To achieve intracellular low Ca^{2+} levels, cells were incubated in Ringer solution with strongly reduced (nominal 50 nM) Ca^{2+} concentration at least 10 min prior to the recordings. The pipette solution contained a nominal free Ca^{2+} concentration of 1 µM.

(A) After establishing the whole-cell configuration and flooding the cells with Ca^{2+}, K^+ currents of increasing amplitudes were recorded during voltage ramps which were applied every 5 s, demonstrating the functional expression of the WT KCNN3 channel and all four channel mutants. The I/V plots show an overlay of subsequently recorded current traces till saturation of current amplitudes. As indicated in the left plot, the vertical bar always applies to 1 nA.

(B) Time course of relative current amplitudes at 0 mV ramp potential. Data correspond to the exemplary current traces shown in (A) (same color code); currents were normalized to the respective maximal current amplitudes. The dotted red lines indicate the two parameters used to characterize and analyze the time course of increasing KCNN3 channel activation: the relative current amplitude I_{10} determined at $t = 10$ s, and the time to reach at least 70% of the maximal current amplitude. Experiments were performed in two sets, each comparing WT channels with two different channel mutants (see Material and Methods).

(C and D) Boxplots of the relative current amplitude I_{10} (C) and the time to reach at least 70% of the maximal current amplitude (D). Whiskers indicate the 10/90 percentiles, and points the 5/95 percentiles. Numbers of experiments are shown in parentheses. Testing for significant differences between median values of groups of one set was performed with the Kruskal-Wallis test (ANOVA on ranks) with post hoc Dunn's test to identify the significantly differing groups. If significant differences were found between channel mutants and WT data, the individual significance level determined with the Wilcoxon-Mann-Whitney test is indicated (**$p < 0.01$, ***$p < 0.001$).

channels (Figure 5). The magnitude of the TBB effect on WT KCNN3 channels ranged from a complete lack of fast current increase (observed in a few cells from both sets of experiments) to about 80-fold potentiation of current amplitudes (2 experiments in set 2).

Simulations of KCNN3 Channel Activity Enable a Quantification of Apparent Ca^{2+} Sensitivity

In order to provide a quantitative interpretation of the significant differences between WT and mutant KCNN3 channels concerning the time course of channel activation in whole-cell experiments and the impaired response to acute TBB application, we simulated current amplitudes of SK channels with various EC_{50} values of apparent Ca^{2+} sensitivity (Figure S5 and Supplemental Note). Comparison of experimental and theoretical data suggests an about 4-fold increase in apparent Ca^{2+} sensitivity of the ZLS-associated mutant channels compared to WT channels in intact cells. Median values obtained for WT KCNN3 experiments agree well with simulations

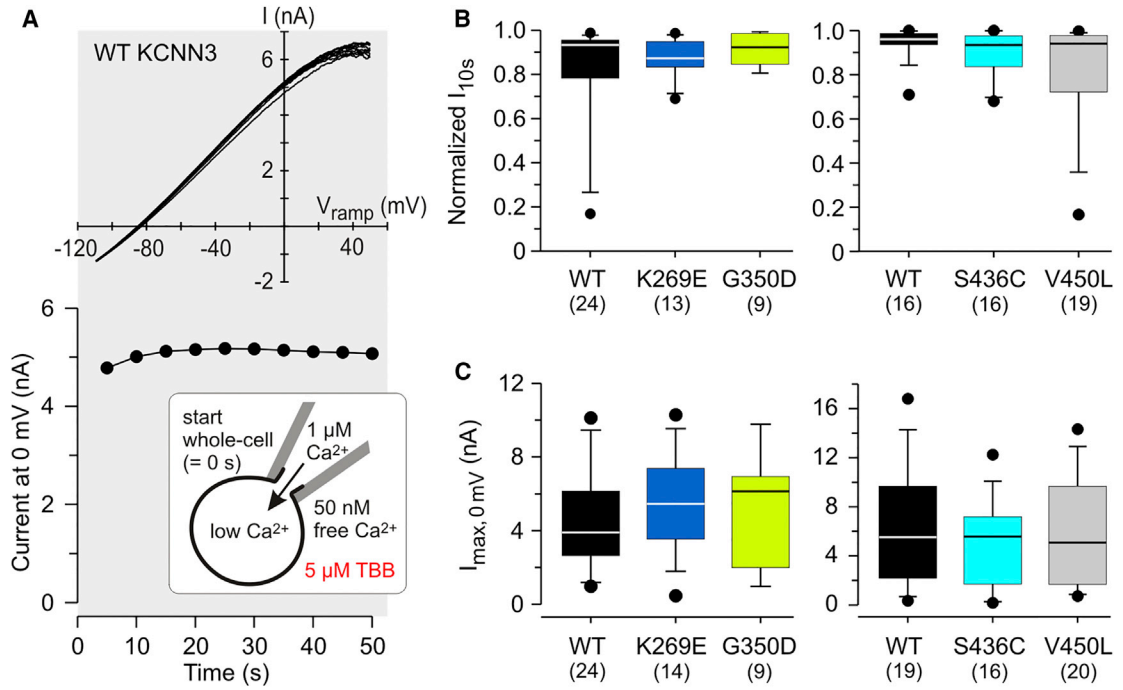

Figure 4. Fast KCNN3 Channel Activation in the Presence of the CK2 Inhibitor TBB
Wild-type (WT), p.Lys269Glu (K269E), p.Gly350Asp (G350D), p.Ser436Cys (S436C), and p.Val450Leu (V450L) KCNN3 whole-cell currents were elicited with voltage ramps from −110 mV to +50 mV with a time interval of 5 s. The pipette solution contained a nominal free Ca^{2+} concentration of 1 μM. Prior to the whole-cell recordings, cells were incubated for at least 5 min in Ringer solution containing the membrane-permeable CK2 inhibitor TBB (5 μM).
(A) As shown for an experiment on WT channels, activation of KCNN3 channels after gaining access to the cell interior was very fast in the continued presence of TBB, resulting in almost maximal current amplitudes upon application of the first voltage ramp. Top: I/V plot with an overlay of current traces elicited by voltage ramps applied every 5 s after whole-cell access. Bottom: time course of the related current amplitude at 0 mV ramp potential.
(B) Boxplots of the relative current amplitude I_{10} determined 10 s after establishment of the whole-cell configuration. Currents were normalized to the maximal current amplitude recorded during the course of the respective experiment.
(C) Boxplots of the maximal current amplitude at 0 mV ramp potential. Whiskers indicate the 10/90 percentiles and points the 5/95 percentiles. Numbers of experiments are shown in parentheses. Statistical analysis with the Kruskal-Wallis test (ANOVA on ranks) yielded no significant differences between groups.

using EC_{50} values around 1.2 μM, whereas median values obtained for the three ZLS-associated KCNN3 mutants are well described by calculations with an EC_{50} value of 0.3 μM (Figures S5B and S5C and Supplemental Note).

The median course of channel activation determined for the KCNN3 channel mutant p.Val450Leu suggests only a slightly increased Ca^{2+} sensitivity compared to WT channels with EC_{50} values around 0.8 μM (Figure S5C). Remarkably, the simulations do not describe the initially elevated current values of the p.Val450Leu KCNN3 mutant (Figure 3B). The significantly higher $I_{10\ s}$ values compared to WT channels (see Figure 3C) point to a small basal activity of p.Val450Leu channels independent of Ca^{2+}. This assumption is supported by additional measurements performed with intact cells in the cell-attached configuration which suggested a low level of constitutive p.Val450Leu channel activity with resting levels of intracellular Ca^{2+} (Figures S6A and S6B). In contrast, WT KCNN3 channels and even highly Ca^{2+}-sensitive p.Lys269Glu channels seem to be almost exclusively in the closed state in intact cells with resting low Ca^{2+} levels (Figure S6C), which is consistent with simulated channel activity at the start of whole-cell configuration (Figure S5B, $t = 0$).

Effects of the KCNN3 p.Lys269Glu Mutation on CK2 Activity

Findings in KCNN2 channels[14] suggested an impaired activation of channel-bound CK2 for the KCNN3 mutant p.Lys269Glu. Nevertheless, basal channel inhibition in intact cells by CK2 was demonstrated by significant effects of TBB pre-incubation. Given the assumed high Ca^{2+} sensitivity of all three ZLS-associated KCNN3 mutants, the observed lack of response to acute TBB application of the p.Lys269Glu mutant cannot serve as a proof of diminished sensitivity to CK2, since highly Ca^{2+}-sensitive SK channels should be almost maximally activated at the time of TBB application (Figure S5 and Supplemental Note). Previously, the Ca^{2+} sensitivity of KCNN2 channels was found to be decreased by applying high Mg-ATP for a few minutes to the cytoplasmic side of the membrane to stimulate CK2 activity.[15] Therefore, we tested the effect of high Mg^{2+} and ATP concentrations in the pipette solution on WT and p.Lys269Glu channel activation

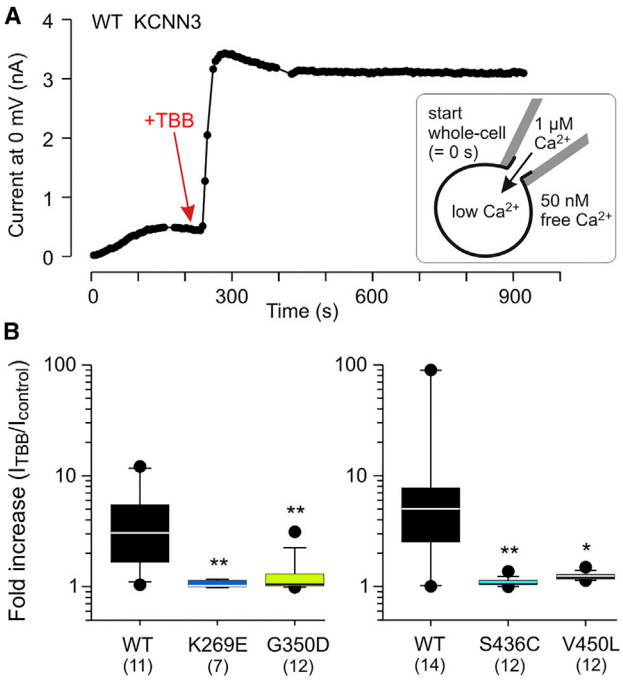

Figure 5. KCNN3 Channel Mutants Show an Impaired Response to Acute TBB Application

Wild-type (WT), p.Lys269Glu (K269E), p.Gly350Asp (G350D), p.Ser436Cys (S436C), and p.Val450Leu (V450L) KCNN3 whole-cell currents were elicited with voltage ramps from −110 mV to +50 mV with a time interval of 5 s. The pipette solution contained a nominal free Ca^{2+} concentration of 1 μM. The CK2 inhibitor TBB (5 μM) was bath-applied after the first saturation of current amplitudes.

(A) Example of the TBB effect on WT KCNN3 channels, illustrating a fast and sustained increase in current amplitude measured at 0 mV ramp potential.

(B) The effect of TBB application was measured as fold current increase in a time window of 150 s starting after TBB application (for details, see Material and Methods). Relative current amplitudes (I_{TBB} / $I_{control}$) are presented as boxplots (whiskers indicate the 10/90 percentiles and points the 5/95 percentiles; the median is shown as line). All mutant channels exhibited a significantly smaller response to TBB compared to WT KCNN3 channels. Please note the logarithmic scale of the TBB effect and the high variability of the TBB effect on WT channels. To test for significant differences between groups, the Kruskal-Wallis test was used with post hoc Dunn's test to identify the significantly differing groups. Individual significance levels of differences between channel mutants and WT data were determined with the Wilcoxon-Mann-Whitney test (*$p < 0.05$, **$p < 0.01$). Numbers of experiments are shown in parentheses.

(Figure S7). Similar to experiments without ATP in the pipette, p.Lys269Glu channels showed a significantly faster initial channel activation than WT channels (Figures S7A–S7C). In contrast to the sustained activation of p.Lys269Glu channels, WT currents were only transiently activated, resulting in significantly smaller relative current amplitudes 5 min after establishing the whole-cell configuration (Figure S7D). Considering the effects of high Mg-ATP on KCNN2/SK2 channels,[14] the transient nature of WT channel activation could be explained by ATP-induced CK2 activation followed by channel-bound CaM phosphorylation leading to a decrease in Ca^{2+} sensitivity of KCNN3. The sustained activation of KCNN3 p.Lys269Glu channels may point to a lower ability of the mutant channel to stimulate CK2 activity.

To address the question of whether diminished CK2 activity leads to reduced CaM phosphorylation and thereby to an increase in Ca^{2+} sensitivity of the KCNN3 p.Lys269Glu channel, we co-expressed HA-tagged KCNN3 wild-type or the p.Lys269Glu mutant together with EYFP-CaM and both the catalytic α (FLAG-tagged) and the regulatory β subunit (Myc-tagged) of CK2[36] in HEK293T cells. Before lysis, cells were incubated in PBS without Ca^{2+} or PBS with Ca^{2+} for 30 min, the latter to enable activation of KCNN3 channels. To determine the amount of phosphorylated CaM, we precipitated EYFP-CaM in IP buffer with or without Ca^{2+} and detected phosphorylated CaM in the immunoprecipitates. We detected no differences in the amount of phosphorylated CaM upon co-expression of wild-type or the KCNN3 p.Lys269Glu mutant in the absence or presence of Ca^{2+} (Figures S8A–S8D).

Discussion

In this work, we provide genetic and functional evidence that *de novo* gain-of-function mutations in *KCNN3* leading to increased Ca^{2+} sensitivity of the encoded mutant channel are implicated in ZLS, similar to monoallelic activating mutations in *KCNH1*.[5] Simulations of KCNN3 channel activity enabled a quantification of our functional whole-cell data and suggested an about 4-fold increase in apparent Ca^{2+} sensitivity of the ZLS-associated KCNN3 mutant channels compared to WT channels in intact cells.

Possible Mechanisms Underlying Enhanced Ca^{2+} Sensitivity of ZLS-Associated KCNN3 Mutant Channels

We can envision different mechanisms for the mutations enhancing the Ca^{2+} sensitivity of the KCNN3 channel. The mutation affecting lysine 269 (p.Lys269Glu) is located in the KCNN3 N terminus. The N terminus of KCNN2 contains the CK2 binding site and a cluster of positively charged residues, including lysine 121.[14] Phosphorylation of CaM by CK2 causes a shift in the Ca^{2+} sensitivity toward an apparently lower sensitivity and speeds up channel deactivation.[15] Therefore, the observed left-shift in the apparent Ca^{2+} sensitivity of KCNN2 K121A channels suggested a role of Lys121 in activation of channel-bound CK2.[14] The N-terminal region of KCNN2 required for CK2 binding is highly homologous in KCNN3, and Lys121 in KCNN2 corresponds to Lys269 in KCNN3. Similar to KCNN2 K121A channels, the increase in Ca^{2+} sensitivity of the KCNN3 p.Lys269Glu mutant channel suggests that replacement of a positively charged residue with a negatively charged one at this position may negatively influence the activity of KCNN3-bound CK2 and thereby indirectly regulate Ca^{2+} sensitivity and channel gating. Our biochemical data, however, did not reveal diminished CaM phosphorylation upon expression of

KCNN3 p.Lys269Glu mutant channels in the absence or presence of Ca^{2+}. These findings may suggest that lysine 269 in KCNN3 (and possibly also lysine 121 in KCNN2) is not critically involved in modulating channel-bound CK2 activity and other mechanisms likely account for increased Ca^{2+} sensitivity of the respective KCNN3 and KCNN2 mutant channels.

According to the KCNN4 channel structure,[27] the two mutated residues Gly350 and Ser436 are located at contact sites between the KCNN3 channel and CaM, with glycine 350 located in the S2-S3 linker and serine 436 in the $S_{45}A$ helix. The S4-S5 linker and especially serine 181 (serine 436 in KCNN3) in the $S_{45}A$ helix have been shown to be crucial for the Ca^{2+}-dependent activation of KCNN4.[27] If the gating mechanism of KCNN4 and KCNN3 is identical, the KCNN3 mutations p.Gly350Asp and p.Ser436Cys may stabilize the interaction of the S2-S3 or the S4-S5 linker with the CaM-binding domain of the channel or directly with CaM to increase the Ca^{2+} sensitivity of the channel. In KCNN2, the p.Val407Phe mutation in the intrinsically disordered fragment (Glu404-Met412) of the C-terminal end also caused an increase in the Ca^{2+} sensitivity of the channel. This amino acid change has been proposed to enhance hydrophobic interactions between the C-terminal CaM binding domain and the S4-S5 linker of the channel,[37] a mechanism that may be similar to the effect of the p.Gly350Asp and p.Ser436Cys amino acid substitutions in KCNN3.

Dominantly acting missense mutations in *KCNN4* have been reported in hereditary xerocytosis, a congenital hemolytic anemia characterized by primary erythrocyte dehydration.[33,38,39] Among the three *KCNN4* mutations linked to hereditary xerocytosis, p.Arg352His is in the CaM-binding (CaMB) domain and p.Val282Met and p.Val282Glu affect the same residue in the pore-forming transmembrane segment S6. All three *KCNN4* mutations result in a gain of function,[40] but the KCNN4 mutant p.Arg352His has been analyzed in more detail using patch-clamp experiments.[33,38,39] Interestingly, similar to the ZLS-associated *KCNN3* mutations reported here, KCNN4 p.Arg352His exhibited an increased Ca^{2+} sensitivity combined with increases in current density and faster activation during whole-cell experiments. It has been speculated that the mutation, which removes a positive charge in the CaMB domain, modifies the interaction with CaM resulting in a more active channel.[33] Taken together, different gain-of-function mutations in both *KCNN3* and *KCNN4* can lead to enhanced Ca^{2+} sensitivity of the encoded channels; however, due to the complex modulation of SK channels by their binding partners CaM, CK2, and PP2A, elucidation of the underlying pathophysiological mechanisms requires more extensive studies in the future.

Physiological Determinants of KCNN3 Ca^{2+} Sensitivity in Intact Cells

In our KCNN3 WT experiments, potentiation of maximal current amplitudes by acute TBB application as well as the time course of channel activation during intracellular Ca^{2+} loading were well described by a major population of channels with EC_{50} values of apparent Ca^{2+} sensitivity around 1.2 μM—with or without an initial state of even lower Ca^{2+} sensitivity (Supplemental Note and Figure S5C). EC_{50} values around 1.2 μM are similar to published data on KCNN2 channels with CaM phosphorylated by CK2,[15] and indeed, CHO cells exhibit high endogenous CK2 sensitivity.[41] Delayed changes in WT KCNN3 current amplitudes observed during prolonged stable whole-cell recordings likely mirror changes in Ca^{2+} sensitivity. Starting with the physiological intracellular environment of an intact cell, the concentration of important cytosolic factors change during the course of the experiments. For example, in addition to calmodulin phosphorylation, binding of phosphatidylinositol-4,5-bisphosphat (PIP2) to KCNN3 might affect its Ca^{2+} sensitivity, because PIP2 has recently been shown to act as a cofactor in Ca^{2+}-dependent KCNN2 channel gating, and PIP2 binding to the KCNN2 channel is hampered by high CK2 activity.[42] A washout of ATP not only reduces CK2 activity, but leads to decreased PIP2 levels in the membrane due to PIP2 dephosphorylation.[43] Thus, complex cell-intrinsic regulation of the Ca^{2+} sensitivity of SK channels impedes experimental determination of physiologically significant EC_{50} values.

The KCNN3 Mutation p.Val450Leu Associated with Portal Hypertension

We characterized not only the effects of the three ZLS-associated *KCNN3* mutations, but also those of the p.Val450Leu change identified in a family with portal hypertension.[32] In contrast to the three ZLS-associated mutants, the KCNN3 p.Val450Leu mutant channel showed only a slight increase in the apparent Ca^{2+} sensitivity. Nevertheless, our data demonstrate a basal constitutive activity of the p.Val450Leu mutant channel with very low Ca^{2+} levels. This finding indicates a different gain-of-function mechanism of the *KCNN3* p.Val450Leu mutation compared to the *KCNN3* p.Lys269Glu, p.Gly350Asp, and p.Ser436Cys variants and explains why different mutations underlie the two non-overlapping *KCNN3*-associated human diseases.

The KCNN3 p.Val450Leu mutation is located in the $S_{45}B$ helix that interacts with S6 from the same and a neighboring subunit in KCNN4 channels, and a conformational change in the S4-S5 linker upon Ca^{2+}-dependent binding of the CaM N-lobe has been suggested to open the channel pore.[27] It is possible that the p.Val450Leu mutation exerts a qualitatively similar effect on the KCNN3 channel pore, even in the absence of Ca^{2+}, resulting in constitutive channel activity.

How could a small basal activity of KCNN3 p.Val450Leu channels cause portal hypertension? Intrahepatic vascular obstruction and increased splanchnic blood flow have been suggested to explain portal hypertension.[44] Whether KCNN3 activity is required for endothelial vasoregulation

in the portal vein, hepatic artery, or sinusoids is not yet known. However, K^+ efflux through ion channels has been shown to regulate liver cell metabolism. In hepatoma cells, metabolic stress leads to opening of SK channels that is beneficial for cell recovery. However, sustained release of K^+ would impair transmembrane cation gradients and may cause enhanced stress in liver cells.[45] In line with this, increased KCNN4 expression was identified in fibrotic liver tissue and activated hepatic stellate cells.[46] By inhibiting KCNN4 channel activity in bile duct ligated rats, portal perfusion pressure could be reduced.[46] Together, these data suggest an important role of Ca^{2+}-dependent K^+ channels in the homeostasis of liver cells. Sustained basal K^+ conductance, as observed for the KCNN3 p.Val450Leu mutant channel, may stress liver cells and lead to portal hypertension and/or liver fibrogenesis.

Increased KCNN3 Channel Function or Expression Negatively Affects Cognitive Function

KCNN3 expression is high in specific regions of the brain, such as the hippocampus, amygdala, and thalamus,[47] and most dopamine-containing cells express KCNN3.[48] In neurons, KCNN3 is involved in the regulation of excitability and firing patterns, neurotransmitter release, and synaptic plasticity.[13,47,49] Increased KCNN3 expression in the hippocampus of aged mice contributes to deficits in hippocampus-dependent memory tasks.[50] Although absence of Kcnn3 did not cause obvious phenotypic anomalies in mice,[51] conditional *Kcnn3*-deficient mice showed altered emotional behavior and selective cognitive defects.[52,53] Similarly, Kcnn3-overexpressing mice presented with deficits in long-term potentiation in the hippocampus and impairment of recognition memory[54] as well as reduction in higher cognitive abilities.[55] These findings demonstrate balanced K^+ channel activities to be critical for normal neurodevelopment and cognition in mice. Cognitive effects of abnormal K^+ channel function also occur in humans (this work, Kortüm et al.,[5] Simons et al.,[6] and Bauer et al.[11]). Further, our *in vitro* data showing increased KCNN3 channel function due to dominantly acting missense mutations in ZLS-affected individuals with mild to moderate intellectual disability underscore the postulated inverse correlation between KCNN3 conductance and high cognitive functions.[55] Accordingly, by normalizing KCNN3 conductance through pharmacological treatment, cognitive function may improve in individuals with *KCNN3* gain-of-function mutation.

Possible Biological Mechanisms Underlying Clinical Features in Subjects with *KCNN3* or *KCNH1* Mutation

Besides cognitive impairment, clinical features of ZLS-affected subjects include distal digital hypoplasia with aplastic or hypoplastic nails and terminal phalanges. The proposed vascular origin for distal digital hypoplasia should be considered in light of KCNN3's role in endothelium-mediated vasodilation.[56,57] The combined function of KCNN3 and KCNN4 channels translates endothelial Ca^{2+} dynamics into changes in vascular tone and blood pressure.[57–60] KCNN3's activity in vascular endothelial cells is highly localized and required to hyperpolarize endothelial cells resulting in smooth muscle cell relaxation and subsequent vascular dilation.[56,57] In mesenteric arteries from spontaneously hypertensive rats, endothelial KCNN3 channel activation and downstream hyperpolarizing pathways were compromised, likely causing an increased vascular tone and elevated blood pressure.[61] These data suggest that local activity of KCNN3 is required in subspaces of endothelial cells to regulate vascular flow.[56,57] It is tempting to speculate that during critical stages of human embryonic development, excessive sustained K^+ conductance due to significantly increased Ca^{2+} sensitivity of mutant KCNN3 channels leads to exaggerated arterial vasodilation, thereby strongly increasing the capillary hydrostatic pressure and causing edema. Vascular ruptures and/or tissue damage in critical phases of organogenesis may result in distal digital hypoplasia in subjects with gain-of-function *KCNN3* mutations. Different endothelial functions of KCNN3 and KCNN4 could explain why gain-of-function mutations in *KCNN4* and *KCNN3* do not converge on the same phenotype in the respective individuals: while acetylcholine-induced vasodilation strongly involves KCNN4, shear stress- and muscular contraction-induced vasodilation mainly depends on KCNN3 channel activation.[58,62]

The possible link between vascular dilation and distal digital hypoplasia is further supported by specific teratogenic effects of antiepileptic drugs.[63,64] Morphological anomalies of the "hydantoin syndrome" like digital hypoplasia have striking similarities with those observed in ZLS-affected individuals.[65] Experiments mainly performed on pregnant rats and rabbits elucidated a common mechanism by which certain anticonvulsants,[66] vasodilators,[67] and hypoxic events[68] induce similar digital anomalies. When applied to the pregnant rats and rabbits during a critical phase of organogenesis, e.g., development of the limb plates, these procedures resulted in (hypoxia-induced) blood vessel dilation, edema, hemorrhage, and finally necrosis of the most distal digital areas in the fetuses.[67] Although no data on endothelial expression of KCNN3 in the developing vascular system exist, its important role in vasodilation suggests that human embryos with gain-of-function *KCNN3* mutations are at risk for vascular damage during limb development resulting in distal digital hypo- or aplasia. Interestingly, the genetically heterogenous Adams-Oliver syndrome was initially reported to have a vascular origin,[69] and more recent data link vascular anomalies to dysregulation of cilia-mediated signaling (see below).[70–72]

KCNH1, another gene mutated in ZLS,[5] plays a role in cell cycle control and proliferation.[73,74] KCNH1 expression occurs during the transition from the G2 phase to mitosis.[75] At the G2/M transition, the cell's cilium is disassembled, a prerequisite for mitosis.[76] KCNH1 localizes to the base of the primary cilium during G2/M transition.

Depletion of KCNH1 causes significant reduction in cilia resorption and delay in proliferation. Conversely, exogenous expression of wild-type KCNH1 in primary mouse embryonic fibroblasts (MEFs) of *Kcnh1* knockout mice reduced the fraction of cells with primary cilia, and the ZLS-associated KCNH1 mutant p.Leu352Val further reduced the cilia frequency.[77] The authors hypothesized that KCNH1 hyperactivity due to activating mutations induces skeletal and nail malformations through altering signaling pathways involved in morphogenesis.[77,78] A similar mechanism was postulated for Ellis-van Creveld syndrome, which includes nail dysplasia and skeletal anomalies. The proteins encoded by *EVC* and *EVC2* localize to the base of cilia and promote hedgehog signaling. Loss of EVC or EVC2 disturbs transmission of the cilia-mediated hedgehog signal.[79,80] Interestingly, the sonic hedgehog pathway is hyperactive in *Kcnh1* knockout MEFs.[77] Cell cycle-dependent expression and a function of KCNN3 in cell cycle progression have not been identified, making it necessary to further investigate the role of SK family members in the cell cycle and/or primary cilium disassembly.

KCNH1-, *KCNK4*-, and *KCNN3*-Related Disorders Define a Subgroup of K^+ Channelopathies

With the identification of gain-of-function mutations in *KCNN3*, we propose to combine the phenotypes associated with mutations in *KCNH1*, *KCNK4*, and *KCNN3* in a subgroup of neurological potassium channelopathies characterized by DD/ID, coarse facial features, and gingival hyperplasia as common findings and epilepsy, hypertrichosis, and nail aplasia or hypoplasia as variable manifestations. This group of disorders is associated with an increase in K^+ conductance, especially evident at negative membrane potentials. Most often, this effect results in more negative resting membrane potentials silencing excitable cells. Nevertheless, excessive sustained K^+ conductance may also result in cellular K^+ depletion and an increase in interstitial K^+ concentration with a depolarizing effect (e.g., on neurons) or a hyperpolarizing effect (e.g., on vascular smooth muscle cells) on neighboring cells. Further studies are required to characterize the effects of increased K^+ conductance on the different tissues and cells in subjects with the disease-relevant mutations.

Supplemental Data

Supplemental Data can be found online at https://doi.org/10.1016/j.ajhg.2019.04.012.

Acknowledgments

We thank all subjects and family members for their participation in this study, Christine Brinker, Annett Hasse, and Inka Jantke for skillful technical assistance, and Hans-Jürgen Kreienkamp for technical advice and helpful discussion. This work was supported by grants from the Deutsche Forschungsgemeinschaft (KO 4576/1-2 to F.K. and K.K.), the Federal Ministry of Education and Research (01DQ17003 to K.K.), and the Canadian Institutes of Health Research to P.M.C. and the Fonds de Recherche du Québec en Santé to P.M.C.

Declaration of Interests

J.K.-R. is an employee of GeneDx, Inc. All other authors declare no competing interests.

Received: February 12, 2019
Accepted: April 15, 2019
Published: May 30, 2019

Web Resources

1000 Genomes, http://www.internationalgenome.org/
CADD, https://cadd.gs.washington.edu/
ClinVar submission page, https://www.ncbi.nlm.nih.gov/clinvar/submitters/26957/
dbSNP, http://www.ncbi.nlm.nih.gov/projects/SNP
ExAC Browser, http://exac.broadinstitute.org
gnomAD Browser, https://gnomad.broadinstitute.org/
M-CAP, http://bejerano.stanford.edu/MCAP/index.html
NCBI Gene, http://www.ncbi.nlm.nih.gov/gene
NHLBI Exome Sequencing Project (ESP) Exome Variant Server, http://evs.gs.washington.edu/EVS/
OMIM, http://www.omim.org/
REVEL, https://sites.google.com/site/revelgenomics/

References

1. Castori, M., Valiante, M., Pascolini, G., Leuzzi, V., Pizzuti, A., and Grammatico, P. (2013). Clinical and genetic study of two patients with Zimmermann-Laband syndrome and literature review. Eur. J. Med. Genet. *56*, 570–576.
2. Chacon-Camacho, O.F., Vázquez, J., and Zenteno, J.C. (2011). Expanding the phenotype of gingival fibromatosis-mental retardation-hypertrichosis (Zimmermann-Laband) syndrome. Am. J. Med. Genet. A. *155A*, 1716–1720.
3. Laband, P.F., Habib, G., and Humphreys, G.S. (1964). Hereditary Gingival Fibromatosis. Report of an Affected Family with Associated Splenomegaly and Skeletal and Soft-Tissue Abnormalities. Oral Surg. Oral Med. Oral Pathol. *17*, 339–351.
4. Zimmermann, K.W. (1928). Ueber Anomalien des Ektoderms. Vierteljahresschrift Zahnheilkunde. *44*, 419–434.
5. Kortüm, F., Caputo, V., Bauer, C.K., Stella, L., Ciolfi, A., Alawi, M., Bocchinfuso, G., Flex, E., Paolacci, S., Dentici, M.L., et al. (2015). Mutations in KCNH1 and ATP6V1B2 cause Zimmermann-Laband syndrome. Nat. Genet. *47*, 661–667.
6. Simons, C., Rash, L.D., Crawford, J., Ma, L., Cristofori-Armstrong, B., Miller, D., Ru, K., Baillie, G.J., Alanay, Y., Jacquinet, A., et al. (2015). Mutations in the voltage-gated potassium channel gene KCNH1 cause Temple-Baraitser syndrome and epilepsy. Nat. Genet. *47*, 73–77.
7. Mégarbané, A., Al-Ali, R., Choucair, N., Lek, M., Wang, E., Ladjimi, M., Rose, C.M., Hobeika, R., Macary, Y., Temanni, R., et al. (2016). Temple-Baraitser Syndrome and Zimmermann-Laband Syndrome: one clinical entity? BMC Med. Genet. *17*, 42.
8. Fukai, R., Saitsu, H., Tsurusaki, Y., Sakai, Y., Haginoya, K., Takahashi, K., Hubshman, M.W., Okamoto, N., Nakashima, M., Tanaka, F., et al. (2016). De novo KCNH1 mutations in four

patients with syndromic developmental delay, hypotonia and seizures. J. Hum. Genet. *61*, 381–387.
9. Bramswig, N.C., Ockeloen, C.W., Czeschik, J.C., van Essen, A.J., Pfundt, R., Smeitink, J., Poll-The, B.T., Engels, H., Strom, T.M., Wieczorek, D., et al. (2015). 'Splitting versus lumping': Temple-Baraitser and Zimmermann-Laband Syndromes. Hum. Genet. *134*, 1089–1097.
10. Bauer, C.K., and Schwarz, J.R. (2018). Ether-à-go-go K^+ channels: effective modulators of neuronal excitability. J. Physiol. *596*, 769–783.
11. Bauer, C.K., Calligari, P., Radio, F.C., Caputo, V., Dentici, M.L., Falah, N., High, F., Pantaleoni, F., Barresi, S., Ciolfi, A., et al. (2018). Mutations in KCNK4 that Affect Gating Cause a Recognizable Neurodevelopmental Syndrome. Am. J. Hum. Genet. *103*, 621–630.
12. Brohawn, S.G. (2015). How ion channels sense mechanical force: insights from mechanosensitive K2P channels TRAAK, TREK1, and TREK2. Ann. N Y Acad. Sci. *1352*, 20–32.
13. Adelman, J.P., Maylie, J., and Sah, P. (2012). Small-conductance Ca2+-activated K+ channels: form and function. Annu. Rev. Physiol. *74*, 245–269.
14. Allen, D., Fakler, B., Maylie, J., and Adelman, J.P. (2007). Organization and regulation of small conductance Ca2+-activated K+ channel multiprotein complexes. J. Neurosci. *27*, 2369–2376.
15. Bildl, W., Strassmaier, T., Thurm, H., Andersen, J., Eble, S., Oliver, D., Knipper, M., Mann, M., Schulte, U., Adelman, J.P., and Fakler, B. (2004). Protein kinase CK2 is coassembled with small conductance Ca(2+)-activated K+ channels and regulates channel gating. Neuron *43*, 847–858.
16. Xia, X.M., Fakler, B., Rivard, A., Wayman, G., Johnson-Pais, T., Keen, J.E., Ishii, T., Hirschberg, B., Bond, C.T., Lutsenko, S., et al. (1998). Mechanism of calcium gating in small-conductance calcium-activated potassium channels. Nature *395*, 503–507.
17. Altmüller, J., Motameny, S., Becker, C., Thiele, H., Chatterjee, S., Wollnik, B., and Nürnberg, P. (2016). A systematic comparison of two new releases of exome sequencing products: the aim of use determines the choice of product. Biol. Chem. *397*, 791–801.
18. Harms, F.L., Girisha, K.M., Hardigan, A.A., Kortüm, F., Shukla, A., Alawi, M., Dalal, A., Brady, L., Tarnopolsky, M., Bird, L.M., et al. (2017). Mutations in EBF3 Disturb Transcriptional Profiles and Cause Intellectual Disability, Ataxia, and Facial Dysmorphism. Am. J. Hum. Genet. *100*, 117–127.
19. Girisha, K.M., Kortüm, F., Shah, H., Alawi, M., Dalal, A., Bhavani, G.S., and Kutsche, K. (2016). A novel multiple joint dislocation syndrome associated with a homozygous nonsense variant in the EXOC6B gene. Eur. J. Hum. Genet. *24*, 1206–1210.
20. Harms, F.L., Kloth, K., Bley, A., Denecke, J., Santer, R., Lessel, D., Hempel, M., and Kutsche, K. (2018). Activating Mutations in PAK1, Encoding p21-Activated Kinase 1, Cause a Neurodevelopmental Disorder. Am. J. Hum. Genet. *103*, 579–591.
21. McKenna, A., Hanna, M., Banks, E., Sivachenko, A., Cibulskis, K., Kernytsky, A., Garimella, K., Altshuler, D., Gabriel, S., Daly, M., and DePristo, M.A. (2010). The Genome Analysis Toolkit: a MapReduce framework for analyzing next-generation DNA sequencing data. Genome Res. *20*, 1297–1303.
22. Wang, K., Li, M., and Hakonarson, H. (2010). ANNOVAR: functional annotation of genetic variants from high-throughput sequencing data. Nucleic Acids Res. *38*, e164.
23. Retterer, K., Juusola, J., Cho, M.T., Vitazka, P., Millan, F., Gibellini, F., Vertino-Bell, A., Smaoui, N., Neidich, J., Monaghan, K.G., et al. (2016). Clinical application of whole-exome sequencing across clinical indications. Genet. Med. *18*, 696–704.
24. Rogers, M.S., and Strehler, E.E. (2001). The tumor-sensitive calmodulin-like protein is a specific light chain of human unconventional myosin X. J. Biol. Chem. *276*, 12182–12189.
25. Turowec, J.P., Duncan, J.S., French, A.C., Gyenis, L., St Denis, N.A., Vilk, G., and Litchfield, D.W. (2010). Protein kinase CK2 is a constitutively active enzyme that promotes cell survival: strategies to identify CK2 substrates and manipulate its activity in mammalian cells. Methods Enzymol. *484*, 471–493.
26. Fanger, C.M., Rauer, H., Neben, A.L., Miller, M.J., Rauer, H., Wulff, H., Rosa, J.C., Ganellin, C.R., Chandy, K.G., and Cahalan, M.D. (2001). Calcium-activated potassium channels sustain calcium signaling in T lymphocytes. Selective blockers and manipulated channel expression levels. J. Biol. Chem. *276*, 12249–12256.
27. Lee, C.H., and MacKinnon, R. (2018). Activation mechanism of a human SK-calmodulin channel complex elucidated by cryo-EM structures. Science *360*, 508–513.
28. Edgar, R.C. (2004). MUSCLE: multiple sequence alignment with high accuracy and high throughput. Nucleic Acids Res. *32*, 1792–1797.
29. Schwede, T., Kopp, J., Guex, N., and Peitsch, M.C. (2003). SWISS-MODEL: An automated protein homology-modeling server. Nucleic Acids Res. *31*, 3381–3385.
30. Sobreira, N., Schiettecatte, F., Valle, D., and Hamosh, A. (2015). GeneMatcher: a matching tool for connecting investigators with an interest in the same gene. Hum. Mutat. *36*, 928–930.
31. Lek, M., Karczewski, K.J., Minikel, E.V., Samocha, K.E., Banks, E., Fennell, T., O'Donnell-Luria, A.H., Ware, J.S., Hill, A.J., Cummings, B.B., et al.; Exome Aggregation Consortium (2016). Analysis of protein-coding genetic variation in 60,706 humans. Nature *536*, 285–291.
32. Koot, B.G., Alders, M., Verheij, J., Beuers, U., and Cobben, J.M. (2016). A de novo mutation in KCNN3 associated with autosomal dominant idiopathic non-cirrhotic portal hypertension. J. Hepatol. *64*, 974–977.
33. Rapetti-Mauss, R., Lacoste, C., Picard, V., Guitton, C., Lombard, E., Loosveld, M., Nivaggioni, V., Dasilva, N., Salgado, D., Desvignes, J.P., et al. (2015). A mutation in the Gardos channel is associated with hereditary xerocytosis. Blood *126*, 1273–1280.
34. Balut, C.M., Hamilton, K.L., and Devor, D.C. (2012). Trafficking of intermediate (KCa3.1) and small (KCa2.x) conductance, Ca(2+)-activated K(+) channels: a novel target for medicinal chemistry efforts? ChemMedChem *7*, 1741–1755.
35. Gao, Y., Balut, C.M., Bailey, M.A., Patino-Lopez, G., Shaw, S., and Devor, D.C. (2010). Recycling of the Ca2+-activated K+ channel, KCa2.3, is dependent upon RME-1, Rab35/EPI64C, and an N-terminal domain. J. Biol. Chem. *285*, 17938–17953.
36. Nuñez de Villavicencio-Diaz, T., Rabalski, A.J., and Litchfield, D.W. (2017). Protein Kinase CK2: Intricate Relationships within Regulatory Cellular Networks. Pharmaceuticals (Basel) *10*, E27.
37. Nam, Y.W., Baskoylu, S.N., Gazgalis, D., Orfali, R., Cui, M., Hart, A.C., and Zhang, M. (2018). A V-to-F substitution in SK2 channels causes Ca^{2+} hypersensitivity and improves locomotion in a C. elegans ALS model. Sci. Rep. *8*, 10749.

38. Glogowska, E., Lezon-Geyda, K., Maksimova, Y., Schulz, V.P., and Gallagher, P.G. (2015). Mutations in the Gardos channel (KCNN4) are associated with hereditary xerocytosis. Blood *126*, 1281–1284.
39. Andolfo, I., Russo, R., Manna, F., Shmukler, B.E., Gambale, A., Vitiello, G., De Rosa, G., Brugnara, C., Alper, S.L., Snyder, L.M., and Iolascon, A. (2015). Novel Gardos channel mutations linked to dehydrated hereditary stomatocytosis (xerocytosis). Am. J. Hematol. *90*, 921–926.
40. Rapetti-Mauss, R., Soriani, O., Vinti, H., Badens, C., and Guizouarn, H. (2016). Senicapoc: a potent candidate for the treatment of a subset of hereditary xerocytosis caused by mutations in the Gardos channel. Haematologica *101*, e431–e435.
41. Wang, H., Yu, S., Davis, A.T., and Ahmed, K. (2003). Cell cycle dependent regulation of protein kinase CK2 signaling to the nuclear matrix. J. Cell. Biochem. *88*, 812–822.
42. Zhang, M., Meng, X.Y., Cui, M., Pascal, J.M., Logothetis, D.E., and Zhang, J.F. (2014). Selective phosphorylation modulates the PIP2 sensitivity of the CaM-SK channel complex. Nat. Chem. Biol. *10*, 753–759.
43. Suh, B.C., and Hille, B. (2008). PIP2 is a necessary cofactor for ion channel function: how and why? Annu. Rev. Biophys. *37*, 175–195.
44. Schouten, J.N., Verheij, J., and Seijo, S. (2015). Idiopathic noncirrhotic portal hypertension: a review. Orphanet J. Rare Dis. *10*, 67.
45. Wang, Y., Sostman, A., Roman, R., Stribling, S., Vigna, S., Hannun, Y., Raymond, J., and Fitz, J.G. (1996). Metabolic stress opens K+ channels in hepatoma cells through a Ca2+- and protein kinase calpha-dependent mechanism. J. Biol. Chem. *271*, 18107–18113.
46. Freise, C., Heldwein, S., Erben, U., Hoyer, J., Köhler, R., Jöhrens, K., Patsenker, E., Ruehl, M., Seehofer, D., Stickel, F., and Somasundaram, R. (2015). K^+-channel inhibition reduces portal perfusion pressure in fibrotic rats and fibrosis associated characteristics of hepatic stellate cells. Liver Int. *35*, 1244–1252.
47. Pedarzani, P., and Stocker, M. (2008). Molecular and cellular basis of small–and intermediate-conductance, calcium-activated potassium channel function in the brain. Cell. Mol. Life Sci. *65*, 3196–3217.
48. Sarpal, D., Koenig, J.I., Adelman, J.P., Brady, D., Prendeville, L.C., and Shepard, P.D. (2004). Regional distribution of SK3 mRNA-containing neurons in the adult and adolescent rat ventral midbrain and their relationship to dopamine-containing cells. Synapse *53*, 104–113.
49. Faber, E.S. (2009). Functions and modulation of neuronal SK channels. Cell Biochem. Biophys. *55*, 127–139.
50. Blank, T., Nijholt, I., Kye, M.J., Radulovic, J., and Spiess, J. (2003). Small-conductance, Ca2+-activated K+ channel SK3 generates age-related memory and LTP deficits. Nat. Neurosci. *6*, 911–912.
51. Bond, C.T., Sprengel, R., Bissonnette, J.M., Kaufmann, W.A., Pribnow, D., Neelands, T., Storck, T., Baetscher, M., Jerecic, J., Maylie, J., et al. (2000). Respiration and parturition affected by conditional overexpression of the Ca2+-activated K+ channel subunit, SK3. Science *289*, 1942–1946.
52. Jacobsen, J.P., Redrobe, J.P., Hansen, H.H., Petersen, S., Bond, C.T., Adelman, J.P., Mikkelsen, J.D., and Mirza, N.R. (2009). Selective cognitive deficits and reduced hippocampal brain-derived neurotrophic factor mRNA expression in small-conductance calcium-activated K+ channel deficient mice. Neuroscience *163*, 73–81.
53. Jacobsen, J.P., Weikop, P., Hansen, H.H., Mikkelsen, J.D., Redrobe, J.P., Holst, D., Bond, C.T., Adelman, J.P., Christophersen, P., and Mirza, N.R. (2008). SK3 K+ channel-deficient mice have enhanced dopamine and serotonin release and altered emotional behaviors. Genes Brain Behav. *7*, 836–848.
54. Martin, S., Lazzarini, M., Dullin, C., Balakrishnan, S., Gomes, F.V., Ninkovic, M., El Hady, A., Pardo, L.A., Stühmer, W., and Del-Bel, E. (2017). SK3 Channel Overexpression in Mice Causes Hippocampal Shrinkage Associated with Cognitive Impairments. Mol. Neurobiol. *54*, 1078–1091.
55. Grube, S., Gerchen, M.F., Adamcio, B., Pardo, L.A., Martin, S., Malzahn, D., Papiol, S., Begemann, M., Ribbe, K., Friedrichs, H., et al. (2011). A CAG repeat polymorphism of KCNN3 predicts SK3 channel function and cognitive performance in schizophrenia. EMBO Mol. Med. *3*, 309–319.
56. Sonkusare, S.K., Bonev, A.D., Ledoux, J., Liedtke, W., Kotlikoff, M.I., Heppner, T.J., Hill-Eubanks, D.C., and Nelson, M.T. (2012). Elementary Ca2+ signals through endothelial TRPV4 channels regulate vascular function. Science *336*, 597–601.
57. Yap, F.C., Weber, D.S., Taylor, M.S., Townsley, M.I., Comer, B.S., Maylie, J., Adelman, J.P., and Lin, M.T. (2016). Endothelial SK3 channel-associated Ca2+ microdomains modulate blood pressure. Am. J. Physiol. Heart Circ. Physiol. *310*, H1151–H1163.
58. Brähler, S., Kaistha, A., Schmidt, V.J., Wölfle, S.E., Busch, C., Kaistha, B.P., Kacik, M., Hasenau, A.L., Grgic, I., Si, H., et al. (2009). Genetic deficit of SK3 and IK1 channels disrupts the endothelium-derived hyperpolarizing factor vasodilator pathway and causes hypertension. Circulation *119*, 2323–2332.
59. Köhler, R., Degenhardt, C., Kühn, M., Runkel, N., Paul, M., and Hoyer, J. (2000). Expression and function of endothelial Ca(2+)-activated K(+) channels in human mesenteric artery: A single-cell reverse transcriptase-polymerase chain reaction and electrophysiological study in situ. Circ. Res. *87*, 496–503.
60. Taylor, M.S., Bonev, A.D., Gross, T.P., Eckman, D.M., Brayden, J.E., Bond, C.T., Adelman, J.P., and Nelson, M.T. (2003). Altered expression of small-conductance Ca2+-activated K+ (SK3) channels modulates arterial tone and blood pressure. Circ. Res. *93*, 124–131.
61. Weston, A.H., Porter, E.L., Harno, E., and Edwards, G. (2010). Impairment of endothelial SK(Ca) channels and of downstream hyperpolarizing pathways in mesenteric arteries from spontaneously hypertensive rats. Br. J. Pharmacol. *160*, 836–843.
62. Milkau, M., Köhler, R., and de Wit, C. (2010). Crucial importance of the endothelial K+ channel SK3 and connexin40 in arteriolar dilations during skeletal muscle contraction. FASEB J. *24*, 3572–3579.
63. Barr, M., Jr., Poznanski, A.K., and Schmickel, R.D. (1974). Digital hypoplasia and anticonvulsants during gestation: a teratogenic syndrome? J. Pediatr. *84*, 254–256.
64. Holmes, L.B., Harvey, E.A., Coull, B.A., Huntington, K.B., Khoshbin, S., Hayes, A.M., and Ryan, L.M. (2001). The teratogenicity of anticonvulsant drugs. N. Engl. J. Med. *344*, 1132–1138.
65. Hanson, J.W. (1986). Teratogen update: fetal hydantoin effects. Teratology *33*, 349–353.
66. Danielsson, B.R., Danielson, M., Rundqvist, E., and Reiland, S. (1992). Identical phalangeal defects induced by

phenytoin and nifedipine suggest fetal hypoxia and vascular disruption behind phenytoin teratogenicity. Teratology *45*, 247–258.
67. Danielsson, B.R., Danielson, M., Reiland, S., Rundqvist, E., Dencker, L., and Regård, C.G. (1990). Histological and in vitro studies supporting decreased uteroplacental blood flow as explanation for digital defects after administration of vasodilators. Teratology *41*, 185–193.
68. Leist, K.H., and Grauwiler, J. (1974). Fetal pathology in rats following uterine-vessel clamping on day 14 of gestation. Teratology *10*, 55–67.
69. Swartz, E.N., Sanatani, S., Sandor, G.G., and Schreiber, R.A. (1999). Vascular abnormalities in Adams-Oliver syndrome: cause or effect? Am. J. Med. Genet. *82*, 49–52.
70. Ezratty, E.J., Stokes, N., Chai, S., Shah, A.S., Williams, S.E., and Fuchs, E. (2011). A role for the primary cilium in Notch signaling and epidermal differentiation during skin development. Cell *145*, 1129–1141.
71. Stittrich, A.B., Lehman, A., Bodian, D.L., Ashworth, J., Zong, Z., Li, H., Lam, P., Khromykh, A., Iyer, R.K., Vockley, J.G., et al. (2014). Mutations in NOTCH1 cause Adams-Oliver syndrome. Am. J. Hum. Genet. *95*, 275–284.
72. Ogawa, M., and Okajima, T. (2019). Structure and function of extracellular O-GlcNAc. Curr. Opin. Struct. Biol. *56*, 72–77.
73. Pardo, L.A., and Stühmer, W. (2014). The roles of K(+) channels in cancer. Nat. Rev. Cancer *14*, 39–48.
74. Cázares-Ordoñez, V., and Pardo, L.A. (2017). Kv10.1 potassium channel: from the brain to the tumors. Biochem. Cell Biol. *95*, 531–536.
75. Urrego, D., Movsisyan, N., Ufartes, R., and Pardo, L.A. (2016). Periodic expression of Kv10.1 driven by pRb/E2F1 contributes to G2/M progression of cancer and non-transformed cells. Cell Cycle *15*, 799–811.
76. Pan, J., and Snell, W. (2007). The primary cilium: keeper of the key to cell division. Cell *129*, 1255–1257.
77. Sánchez, A., Urrego, D., and Pardo, L.A. (2016). Cyclic expression of the voltage-gated potassium channel KV10.1 promotes disassembly of the primary cilium. EMBO Rep. *17*, 708–723.
78. Urrego, D., Sánchez, A., Tomczak, A.P., and Pardo, L.A. (2017). The electric fence to cell-cycle progression: Do local changes in membrane potential facilitate disassembly of the primary cilium?: Timely and localized expression of a potassium channel may set the conditions that allow retraction of the primary cilium. BioEssays *39*, 39.
79. Pusapati, G.V., Hughes, C.E., Dorn, K.V., Zhang, D., Sugianto, P., Aravind, L., and Rohatgi, R. (2014). EFCAB7 and IQCE regulate hedgehog signaling by tethering the EVC-EVC2 complex to the base of primary cilia. Dev. Cell *28*, 483–496.
80. Ruiz-Perez, V.L., and Goodship, J.A. (2009). Ellis-van Creveld syndrome and Weyers acrodental dysostosis are caused by cilia-mediated diminished response to hedgehog ligands. Am. J. Med. Genet. C. Semin. Med. Genet. *151C*, 341–351.